



University of Connecticut  
**OpenCommons@UConn**

---

Master's Theses

University of Connecticut Graduate School

---

12-16-2012

# A Finite Difference Implementation of Phase Field Theory

Nicholas W. Oren

*University of Connecticut - Storrs*, [Orenn89@gmail.com](mailto:Orenn89@gmail.com)

---

## Recommended Citation

Oren, Nicholas W., "A Finite Difference Implementation of Phase Field Theory" (2012). *Master's Theses*. 368.  
[https://opencommons.uconn.edu/gs\\_theses/368](https://opencommons.uconn.edu/gs_theses/368)

This work is brought to you for free and open access by the University of Connecticut Graduate School at OpenCommons@UConn. It has been accepted for inclusion in Master's Theses by an authorized administrator of OpenCommons@UConn. For more information, please contact [opencommons@uconn.edu](mailto:opencommons@uconn.edu).

A Finite Difference Implementation of Phase Field  
Theory

Nicholas Waters Oren

B.S., Union College, 2011

A Thesis

Submitted in Partial Fulfillment of the  
Requirements for the Degree of  
Master of Science

at the

University of Connecticut

2012

APPROVAL PAGE

Master of Science Thesis

A Finite Difference Implementation of Phase Field Theory

Presented by

Nicholas Waters Oren, B.S.

Major Advisor \_\_\_\_\_  
Dr. Brice Cassenti

Associate Advisor \_\_\_\_\_  
Dr. Wei Sun

Associate Advisor \_\_\_\_\_  
Dr. Eric Jordan

Associate Advisor \_\_\_\_\_  
Dr. Alexander Staroselsky

University of Connecticut

2012

## Acknowledgements

I would like to thank Pratt & Whitney for their generous support of this research. I would also like to thank my advisor Dr. Brice Cassenti. Dr. Cassenti went above and beyond what is expected from an advisor and was more helpful than I can say. His guidance and encouragement are what really made this project enjoyable and successful. I would like to thank Dr. Alex Staroselsky, from Pratt and Whitney, for his help and support of this work. I would also like to thank Dr. Eric Jordan for kindly allowing me to work in his lab for the duration of my time working on this project, as well as for being an associate advisor to this thesis. I would also like to thank Dr. Wei Sun for being an associate advisor to this thesis as well. Finally I would like to thank the University of Connecticut's Mechanical Engineering Department for all of the work that they do to insure the best possible experience and education for their graduate students.

## Table of Contents

Table of Figures .....	vi
Abstract .....	viii
Motivation.....	1
Background .....	2
Theory .....	7
Test Cases .....	15
Shear Case.....	16
Tension Case.....	17
Finite Difference Code.....	21
Finite Difference Formulation .....	21
Interior Equations.....	22
Sides.....	23
Corners .....	23
Displacement Boundary Conditions .....	25
Phase Finite Difference Representation.....	27
Building the Matrix.....	30
Solving the Matrix .....	32
Applying Equations .....	32
Displacement.....	32
Taylor Series .....	33
Stress Equations .....	34
Interior Stress Equilibrium Equations.....	34

Normal Stress Boundary Conditions .....	35
Shear Stress Boundary Conditions.....	36
Variable Time Step .....	36
Speeding up the Code .....	36
Results.....	41
Shear Results.....	41
Tension Results .....	52
Conclusions and Future Work .....	64
Appendix.....	65
References.....	67

## Table of Figures

Figure 1: Double Well Potential Function with Symmetric Minima <sup>[8]</sup> .....	3
Figure 2: 1-D crack Propagation from Karma Results <sup>[8]</sup> , 2001 .....	4
Figure 3: Phase Field Crack Propagation <sup>[9]</sup> .....	5
Figure 4: Double Well Potential Function .....	12
Figure 5: Derivative of Double Well Potential .....	13
Figure 6: Basic set up of test cases. ....	15
Figure 7: Shear Test Case Set-up.....	17
Figure 8: Tension Test Case Set-up .....	18
Figure 9: Tension Test Case Symmetry .....	19
Figure 10: Symmetry Boundary Conditions .....	20
Figure 11: Interior Nodes.....	22
Figure 12: Side nodes.....	23
Figure 13: Corner Nodes.....	24
Figure 14: Displacement Boundary Conditions.....	25
Figure 15: Location of equations for displacement conditions.....	26
Figure 16: Phase initial conditions.....	27
Figure 17: Shear Test Case Phase B.C.....	28
Figure 18: Tension test case phase B.C. ....	29
Figure 19: Program Flow Chart .....	38
Figure 20: Final Phase of Plate .....	41
Figure 21: Final Shear Stress .....	42
Figure 22: Stress in the X-Direction .....	43

Figure 23: Stress in the Y-Direction .....	44
Figure 24: Maximum Principle Stress .....	45
Figure 25: Diffusion Constant .....	46
Figure 26: Left side of Crack, Min Principle Direction.....	47
Figure 27: Right side of Crack, Min Principle Direction.....	47
Figure 28: Deformation of plate .....	48
Figure 29: Phase with time .....	49
Figure 30: Measured Kink Angle .....	50
Figure 31: Doubled Run Time Crack Growth .....	51
Figure 32: Final phase.....	52
Figure 33: Final shear stress plot .....	53
Figure 34: Final stress-x.....	54
Figure 35: Stress-y .....	55
Figure 36: Maximum Principle Stress .....	56
Figure 37: Diffusion Constant .....	57
Figure 38: Left side of Crack, Min Principle Direction.....	58
Figure 39: Right Side of Crack, Min Principle Direction.....	58
Figure 40: Deformation.....	59
Figure 41: Phase as a function of time.....	60
Figure 42: Stress Intensity Factor Data.....	62
Figure 43: Stress Intensity Comparison.....	63



## **Abstract**

Computationally handling cracks generally results in numerically unstable results. Specifically handling the infinite stresses at the crack tip as well as the abrupt change from virgin material to failed material creates numerical instabilities. This project seeks to determine if phase field physics theory, particularly the theory developed by B. N. Cassenti et al., can be appropriately applied to crack propagation. The method that phase field theory uses is by introducing another state variable, called the phase of the material that represents the level of failed or cracked, and diffuses it along a crack. This new physics based variational principle was tested in this project.

To test this theory, two numerical test cases were modeled using finite difference approximations. The first test applied shear loading creating a mode II fracture. This test case allowed the accuracy of the crack propagation, particularly the kink angle, to be shown. The second test applied tension to a crack in a mode I fracture. This allowed for the rate of the crack growth, as well as the stress intensity factor to be measured and compared to traditional fracture mechanics theory.

Both test cases provided results that could be compared to calculations from fracture mechanics theory. In both cases the results of the phase diffusion and stress distribution aligned with the results from fracture mechanics. From the results presented here it is clear that phase field physics theory can be appropriately applied to cracks. This project has successfully proven that this

theory is ready to be implemented into a finite element program for practical fracture analysis.

.

## Motivation

Predicting the life and failure of single crystal turbine blades is challenging. The current inelastic material model that has been developed at Pratt and Whitney in conjunction with the University of Connecticut has proved difficult to use when cracks are present in single crystal components. The model is numerically difficult to implement and the inclusion of cracks and other singularities make it even more difficult<sup>[1]</sup>. Any fracture mechanics numerical algorithm requires re-meshing in order to handle crack propagation. The phase field method discussed in this thesis avoids these difficulties.

Other methods of brittle fracture only provide accurate results far away from the crack tip. Near the crack tip, additional boundary conditions are inserted to provide driving stresses. These types of solutions give the crack tip a velocity determined by the amount of energy being put into the crack tip<sup>[2,3]</sup>. These methods do not predict the instabilities at the crack tip well nor do they accurately determine the crack tip velocity. Methods of this sort have extreme difficulties handling the instabilities of rapid dynamic crack growth<sup>[4-6]</sup>.

The goal of this work is to develop a numerical implementation of the variational approach developed by B. N. Cassenti et al<sup>[7]</sup>. The finite difference scheme was chosen for the sake of clarity. In order to prove that the theory accurately represents cracks the code should be able to show crack diffusion and growth that is in agreement with fracture mechanics theory. More importantly the code should also show that the numerical stability near the crack has improved.

## Background

In its most basic implementation, phase field physics can be used to increase the numerical stability of singular areas in material models. Numerically, cracks are difficult to model as they have theoretical infinite stresses at their tips, as well as sharp moving boundary conditions between virgin and failed material. The idea behind phase field physics is that instead of having sharp edges of failed and virgin material around the crack, the crack is diffused out into the surrounding material. This allows the material to make a smooth transition from virgin material to fully cracked material as well as removing the infinite stresses that occur at the crack tip. A new state variable is introduced at each node that quantifies the level of damage. The cracked level will be referred to as the phase of the material. The phase is allowed to go between zero and one, zero being fully cracked and one being virgin material. Therefore, by using the phase of the material we can show how cracks grow, as well as make the stress of each node a function of the phase of the node. All that is needed is a way to diffuse the phase correctly. Material properties are explicit functions of the phase indicator, so the change of the stiffness in the cracked area is varied accordingly.

This method has been previously investigated in diverse research by Alain Karma<sup>[8-10]</sup>. Karma has done extensive work using phase field models to predict crack growth. In his paper<sup>[8]</sup>, Phase-Field Model of Mode III Dynamic Fracture, the potential of phase field physics as it relates to crack growth was shown. He sets up a 1-D mode III fracture problem. In equation (1), the author found a three term diffusion equation for phase.

$$\tau d_t \phi(\vec{x}, t) = D_\phi \nabla^2 \phi - V'_{DW}(\phi) - \frac{\mu}{2} g'(\phi) (\bar{\epsilon}^2 - \bar{\epsilon}_c^2) \quad (1)$$

In this equation a double well potential function is used having the form as seen in equation (2).

$$V_{DW}(\phi) = \frac{1}{4} \phi^2 (1 - \phi)^2 \quad (2)$$

A graph of this double well potential function is shown in Figure 1. It is clear from this plot that the same potential is assigned to both the fully cracked state and virgin state.

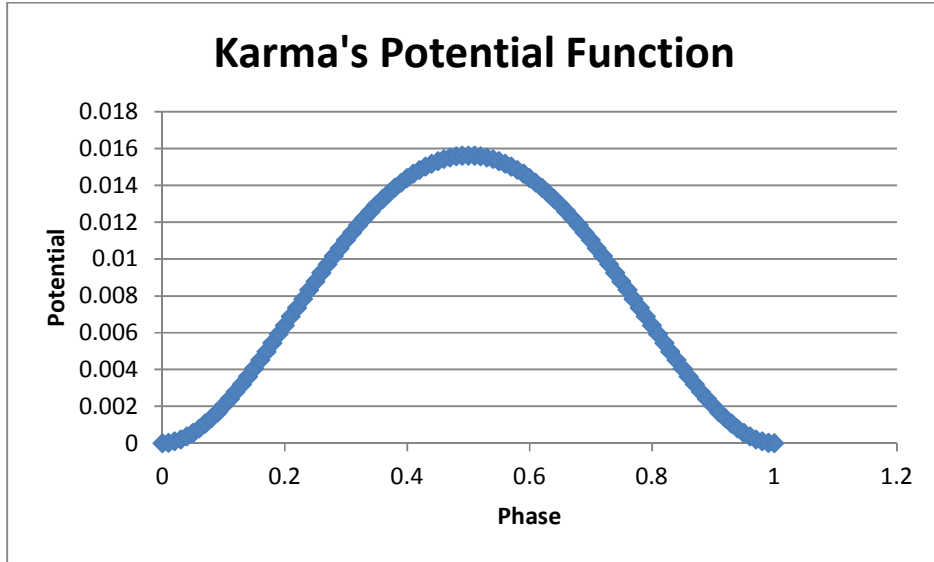


Figure 1: Double Well Potential Function with Symmetric Minima<sup>[8]</sup>

In this paper, a function for  $g(\phi)$  as seen in equation (3) is assumed. This function, when multiplied by the elastic moduli, establishes the evolution of the elastic properties with phase change. Karma assumes:

$$g(\phi) = 4\phi^3 - 3\phi^4 \quad (3)$$

The author then applies his equations to a 1-D strip model and uses a Crank-Nicholson alternating-direction-implicit scheme to test his governing equations.

Figure 2 shows his results from this model:

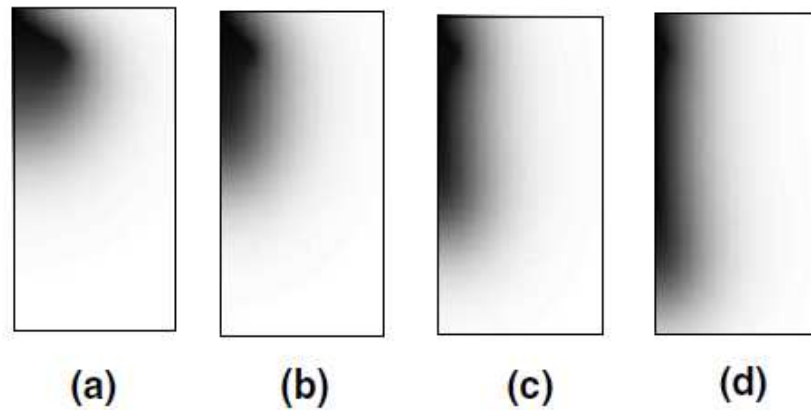


**Figure 2: 1-D crack Propagation from Karma Results<sup>[8]</sup>, 2001**

The results show the phase of the material diffusing and propagating along the left edge of the material. For this model the white corresponds to a phase of 1 and the black corresponds to a phase of 0, and the sub figures, a through d, show the progress with time. These figures show that this approach allows the diffusion of the phase of the material, however the variational principle used by Karma is not entirely physics based.

In the recent publication (Karma 2008)<sup>[9]</sup> there is an attempt to show how phase field physics can accurately determine the kink angles that cracks propagate at as well as their velocities. Again this paper produces results based on his previous paper's variational principle. Figure 3<sup>[9]</sup>, illustrates some results for crack propagation.

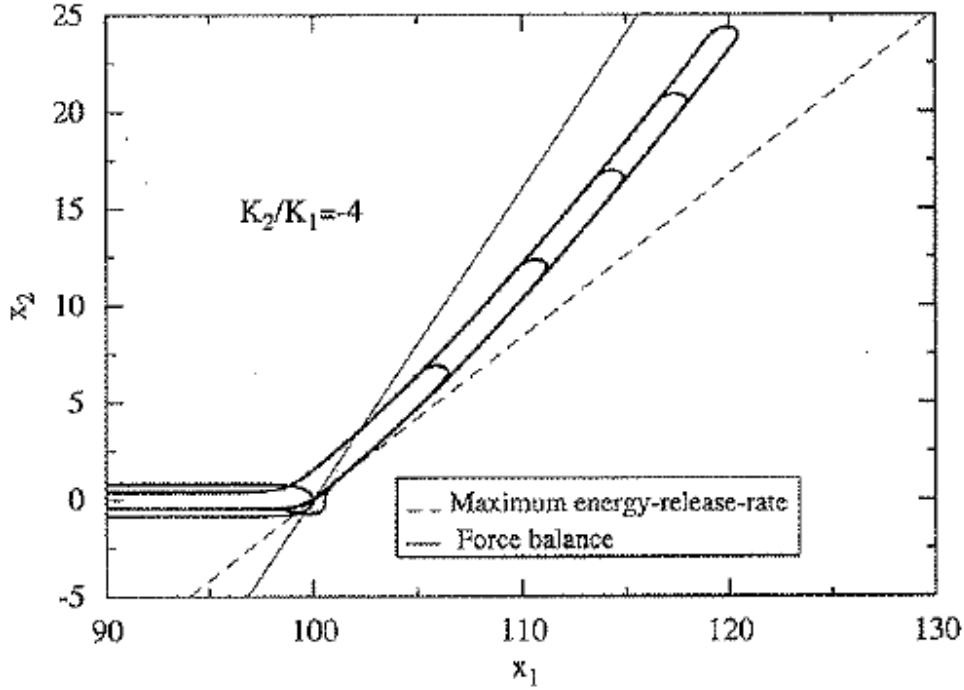


**Figure 3: Phase Field Crack Propagation<sup>[9]</sup>**

In this work the kink angles for crack propagation have been found<sup>[9]</sup>. Figure 3 is the result of a phase field simulation for pure antiplane shear. However, upon closer examination the crack curves upwards as it propagates, which contradicts fracture mechanics. Also in this particular case, in order to propagate the crack at the kink angle, the author simply calculates the angle that the crack should propagate from fracture mechanics, and then enforces the diffusion in that direction. In this sense, the work<sup>[9]</sup> forces the crack in a particular direction instead of allowing the physics to drive the crack propagation.

Producing a physics based variational principle for the diffusion of the phase of the material is critical. In the paper, “A variational formulation of the coupled thermo-mechanical boundary-value problem for general dissipative

solids,” Ortiz shows how to produce a variational principle for the coupled thermo-mechanical problem for dissipative solids<sup>[11]</sup>. This theory assisted in creating the particular theory that was ultimately tested in this work. However, this theory showed how to create a variational principle just in space, and did not include time.



## Theory

### Constants

The notations used are review in Table 1 below.

**Table 1: Parameters and their meanings**

Term	Definition
K	Thermal Conductivity Parameter
K'	Thermal Conductivity Parameter
J'	Diffusion Constant
$\Omega_1$	Vibration Frequency Parameter
$\Omega_2$	Vibration Frequency Parameter
$D_\phi$	Diffusion Coefficient
$C_P$	Specific Heat
$\tau$	Characteristic Time for Diffusion Equation
$\dot{v}$	Random Velocities from Temperature
$\dot{u}$	Random Velocities from Internal Energy
$\alpha$	Double Well Function Constant
m	Parameter for Modifying Modulus
n	Parameter for Modifying Modulus
$\alpha_{kl}$	Thermal Coefficient of Expansion

## Theory

The theoretical basis for the section is described in Ref.[7]. In [7], a physics based Lagrangian is derived that results in a time dependent diffusion equation. The formulation is backed by supporting molecular dynamic simulations<sup>[12,13]</sup>. The Lagrangian density is:

$$\mathcal{L} = \frac{1}{2} \rho \dot{u}_i \dot{u}_i + \frac{1}{2} \rho \dot{u}^2 + \frac{1}{2} \rho \dot{v}^2 - \int \epsilon_{ij} \left( \dot{v}, \dot{u}, \epsilon' \right) d\epsilon'_{ij} - V_{DW}(\phi) - u_i F_i - \frac{1}{2} \tilde{K} \tilde{u}_{,i} \tilde{u}_{,i} - \frac{1}{2} \tilde{J} \tilde{v}_{,i} \tilde{v}_{,i} \quad (4)$$

The parameters and variables can all be related as follows:

$$\tilde{u} = \frac{\dot{\tilde{u}}}{\Omega_0}, \tilde{v} = \frac{\dot{\tilde{v}}}{\Omega_1}, T = \frac{\dot{\tilde{u}}^2}{4c_p}, \phi = \frac{\dot{\tilde{v}}^2}{4(\tau/\rho)}, K' = \frac{\Omega_0 K}{4c_p}, J' = \frac{\Omega_1 D_\phi}{4(\tau/\rho)} \quad (5)$$

In the above equations the  $\dot{\tilde{u}}$  and  $\dot{\tilde{v}}$  terms represents the random velocities.

These displacements and random velocities are separated into two components.

The  $\dot{\tilde{u}}$  component is the random velocity due to temperature. The  $\dot{\tilde{v}}$  component of the random velocity is related to the phase. The Lagrangian contains both the global  $(u_i, v_i)$  and local random components  $(\tilde{u}_i, \tilde{v}_i)$ . The local random terms become zero when averaged over their direction, but they still contain random kinetic and potential energy. Although some random local components contain dot accents, these dots do not represent time derivatives, rather they include different types of energies. That is, terms with dot accents represent the kinetic energy contribution. The terms without the accents represent potential energy.

Next the variation of the action is set to zero. This leads to equation (6), which is the time dependent diffusion equation.

$$\rho \frac{\partial \dot{\tilde{v}}}{\partial t} = (J \tilde{v}_{,i})_{,i} - \frac{1}{2} \frac{\partial J'}{\partial \tilde{v}} \tilde{v}_{,i} \tilde{v}_{,i} - V'_{DW}(\phi) \frac{\partial \phi}{\partial \tilde{v}} - \int^\epsilon \frac{\partial \sigma_{ij}}{\partial \tilde{v}} d\epsilon'_{ij} \quad (6)$$

In this thesis the theory was simplified to make it more computationally friendly. The first simplification that was made is that the elastic waves created are not being tracked; rather a steady state solution is sought. While the elastic waves are indeed propagating though the material, their impacts on the results are minimal. Tracking these waves though the material would be computationally

costly and unnecessary. The next simplification made is that  $J'$  is a constant. As seen in Table 1,  $J'$  is a diffusion constant. It is not a function of the phase of the material so it was assumed that its change with the phase of the material is very small. This allows the second term to be eliminated. The simplified version of the diffusion equation can be seen in equation (7).

$$\rho \frac{\partial \tilde{v}}{\partial t} = (J \tilde{v}_{,i})_{,i} - V'_{DW}(\phi) \frac{\partial \phi}{\partial \tilde{v}} - \int^{\epsilon} \frac{\partial \sigma_{ij}}{\partial \tilde{v}} d\epsilon'_{ij} \quad (7)$$

As one can see, this diffusion equation is reduced to a three term equation. A finite difference code was developed for equation (7) (to update  $\tilde{v}$  at every time step). A forward difference was used for the time derivative and central differences for the spatial derivatives. By using finite difference approximations to expand the time derivative in this equation, it can be written out, in general, as shown in equation (8).

$$\dot{\tilde{v}}_{n+1} = \dot{\tilde{v}}_n + Diff - DW - Strain\_Energy \quad (8)$$

Equation (8) is used to update the phase at every node every time step. The equation can now be discussed term by term. In this version of the equation the terms are replaced with labels to more precisely describe exactly what their role is. This is how the equation is actually broken up in the finite difference model, as it allows the parts to be determined individually, then added together at the end. This equation uses the current phase or  $\tilde{v}$  at the current time step and adds the change in from the other three terms. The other three terms are a diffusion term, a double well potential term, and a strain energy term. In this version of the

equation  $\dot{v}$  is used instead of  $\phi$ .  $\phi$ , or the phase of the material is a function of  $\dot{v}$ , and is related using equation (9).

$$\phi = \frac{\dot{v}^2}{4(\frac{\tau}{\rho})} \quad (9)$$

The first term to be discussed is the diffusion term. This term was used to insure phase diffusion in the direction of the minimum principle stress. The first step to finding this term's value was to build the stress tensor at the current node. Next, the smallest eigenvalue and the corresponding eigenvector of the stress tensor at the current point were found. Then, the sign of the eigenvector dot product with the gradient of  $\phi$  and was multiplied to the eigenvector. This process ensures that only directions that are in line with the gradient of phi are positive. Finally the eigenvectors are all normalized.

Next two coefficients,  $D_I$  and  $D_0$ , were defined.  $D_I$  represents the diffusion coefficient in the direction of the crack growth and  $D_0$  represents isotropic diffusion. Generally  $D_0$  was set to zero, and  $D_I$  was set to a constant times  $e^{((\sigma_{max}-\sigma_{applied})*Constant)}$ . This exponential term allows the diffusion term to be higher in the direction of crack growth as well as be higher near the crack tip. This essentially raises the amount of crack diffusion around the crack tip and increases the diffusion in the direction of crack growth. Next  $D_0$  and  $D_I$  were used in equation (10) to allow different diffusion constants in the different principle directions.

$$D_{ij} = D_0\delta_{ij} + D_I n_i n_j \quad (10)$$

As per indicial notation using this equation, equations (11, 12, and 13) were used to define the two dimensional diffusion tensor containing terms  $D_{11}$ ,  $D_{12}$ , and  $D_{22}$ .

$$D_{11} = D_0 + D_1 n_1^2 \quad (11)$$

$$D_{12} = D_1 n_1 n_2 \quad (12)$$

$$D_{22} = D_0 + D_1 n_2^2 \quad (13)$$

Finally the diffusion term could be written out as seen in equation (14).

$$\frac{d\dot{\psi}}{dt} = D_{11} \frac{d^2 \dot{\psi}}{dx^2} + 2D_{12} \frac{d^2 \dot{\psi}}{dxdy} + D_{22} \frac{d^2 \dot{\psi}}{dy^2} \quad (14)$$

Using finite difference approximations on the differential terms, this equation can be expanded into a forward difference equation.

The next term in the diffusion equation is a double well term. This term either drives the phase of the material to zero or one. Unlike the work by Karma, this potential function was chosen to be more physically acceptable. This component can be thought of as the material being pushed to either its virgin state or its fully failed state. It is easiest to understand the effect of the double well function by inspecting equation (15) and corresponding graph.

$$V_{DW}(\phi) = V_0(1 - \phi)^2(1 + 2\phi + \alpha\phi^2) \quad (15)$$

The graph of this function is seen in Figure 4:

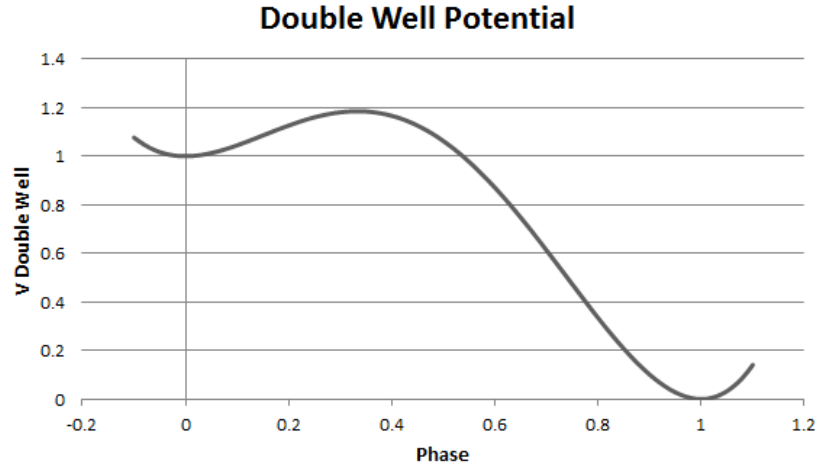


**Figure 4: Double Well Potential Function**

As seen, there are two stable positions for the phase of the material that correspond to local minima's of potential. These are at zero (completely failed) and one (virgin). Also it is important to note that the local minima at zero is higher than the global minima at one. The actual function used in the diffusion equation is the derivative of the double well potential function with respect to  $\phi$  as seen in equation (16).

$$V_{DW}(\phi)' = 2V_0(\phi - 1)\phi(\alpha(2\phi - 1) + 3) \quad (16)$$

The graph of this function is shown in Figure 5:

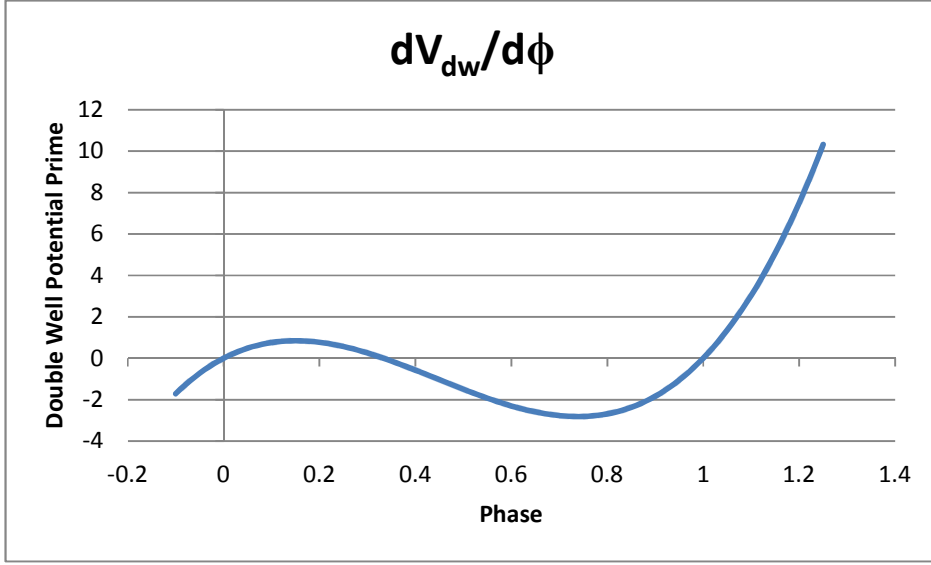


**Figure 5: Derivative of Double Well Potential**

As one can clearly see from Figure 5 the double well potential term will act to hold the phase at zero or one, or push the phase towards zero or one. For example, when the phase is just below one, the term becomes negative, and when it is subtracted in the main diffusion equation, it acts to add to the phase at the next time step; therefore forcing the phase back to 1.

The final term to be discussed is the strain energy term. Since only the variation from  $\tilde{v}$  is sought, the rest of the terms generally associated with strain energy are left out. As seen in the previous diffusion equation the term is:

$$\text{Strain Energy} = \int^{\epsilon} \frac{d\sigma_{ij}}{d\tilde{v}} d\epsilon'_{ij} \quad (17)$$

This term can be expanded into a form that can be easily implemented in the finite difference code using equation (18).

$$\text{Strain Energy} = \Omega_1 g(\phi)' \sqrt{\phi / (\frac{\tau}{\rho})} \left[ \frac{1}{2} \lambda (\epsilon_{xx}^2 + \epsilon_{yy}^2) + \mu (\epsilon_{xy}^2 + \epsilon_{xx}^2 + \epsilon_{yy}^2) \right] \quad (18)$$

Ultimately this term causes the phase to be lower in areas that have high amounts of strain.

It is also important to note that each term in the main diffusion equation is paired with a constant. These constants were tuned in order to give each term its appropriate amount of influence in the equation. This was determined by a trial and error method. Numerically no single term should be able to change the phase by more than 5% in any given single time step.

Equation (19) shows how an elastic modulus scaling function is incorporated. This is used to modify the modulus of the material depending on the phase of the material.

$$\sigma_{ij} = C_{ijkl}^0 g(\phi) [\epsilon_{kl} - \alpha_{kl}(T)(T - T_R) - \epsilon_{kl}^p] \quad (19)$$

For this work, with the simplifying assumptions of constant temperature, equation (19) can be simplified as shown in equation (20).

$$\sigma_{ij} = g(\phi) [\lambda \epsilon_{kk} \delta_{ij} + 2\mu \epsilon_{ij}] \quad (20)$$

As one can see, the stress is now a function of the elastic modulus scaling function. A physically acceptable function for the elastic modulus scaling function is shown in equation (21).

$$g(\phi) = 1 - \frac{(1-\phi)^{m+1}}{n} \left[ (m+n+1) - (m+1)(1+\phi)^n \right] \quad (21)$$

From equation (21) it is clear that  $g$  is a function of the phase of the material. It also incorporates  $m$  and  $n$  as parameters to adjust the shape of the function.



A brief summary of the governing equations can be found in the Appendix.

## Test Cases

Two different test cases were constructed based on the theory. These test cases were designed to simulate mode I and mode II fracture. Each test case was a plate of aluminum that had a crack in the center. Plain strain conditions were assumed, that is the displacement in the z-direction was zero. This essentially made the test cases two dimensional. Figure 6 shows the basic set up of both test cases.

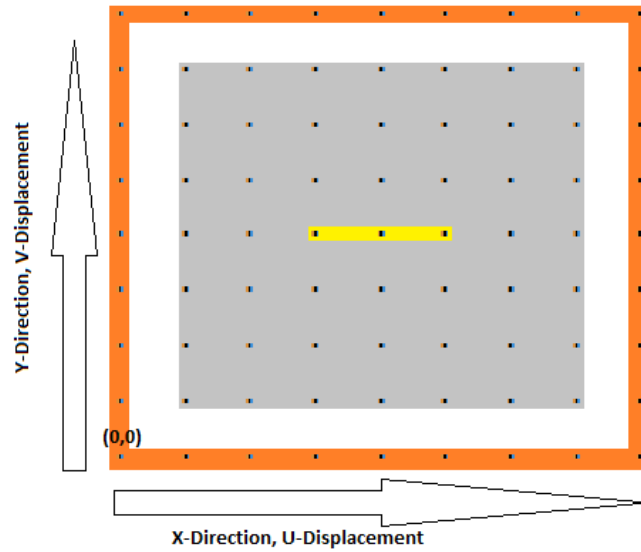


**Figure 6: Basic set up of test cases.**

As seen in Figure 6 the test sample is the gray colored section of the dots. The yellow portion of the dots in the middle is where the crack is initially at  $t = 0$ .

The outer ring of orange dots is referred to as the “n+1” nodes. These are the nodes that contain the information regarding the boundary conditions. Figure 6 also shows the orientation of the coordinate system in the lower left corner.

### **Shear Case**

The shear test case was designed to show that phase field theory could accurately predict the kink angle for crack propagation. The basic setup is the same as shown and discussed previously in Figure 6. All around the sides of the plate, a shear stress was applied, where the normal stresses, around the plate, were set to zero. With these conditions the crack should grow diagonally towards the upper left and lower right corners. Fracture mechanics predicts that the crack should initially propagate at  $69^\circ$  and then turn to propagate at  $45^\circ$ <sup>[18]</sup>. Figure 7 shows the boundary conditions that were applied for the shear test case.

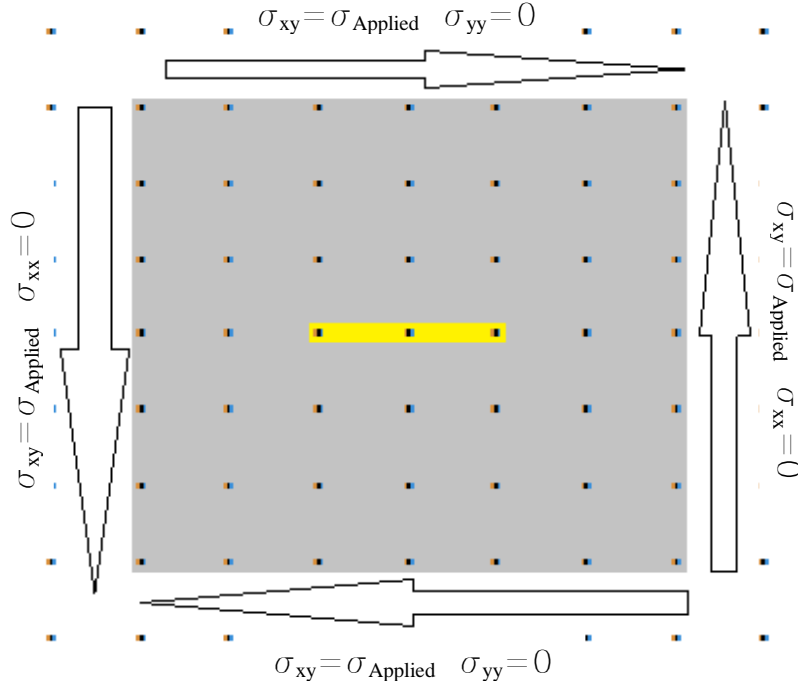


**Figure 7: Shear Test Case Set-up**

### Tension Case

Uniaxial tension was the second case that was designed to test the capabilities of the theory. The interior set up was similar to the shear test case with the interior crack. This time, a normal stress was applied to both the top and the bottom, essentially pulling the plate from the top and bottom. With this test case, the crack is expected to grow straight out towards the sides of the plate. This set up is shown in Figure 8:

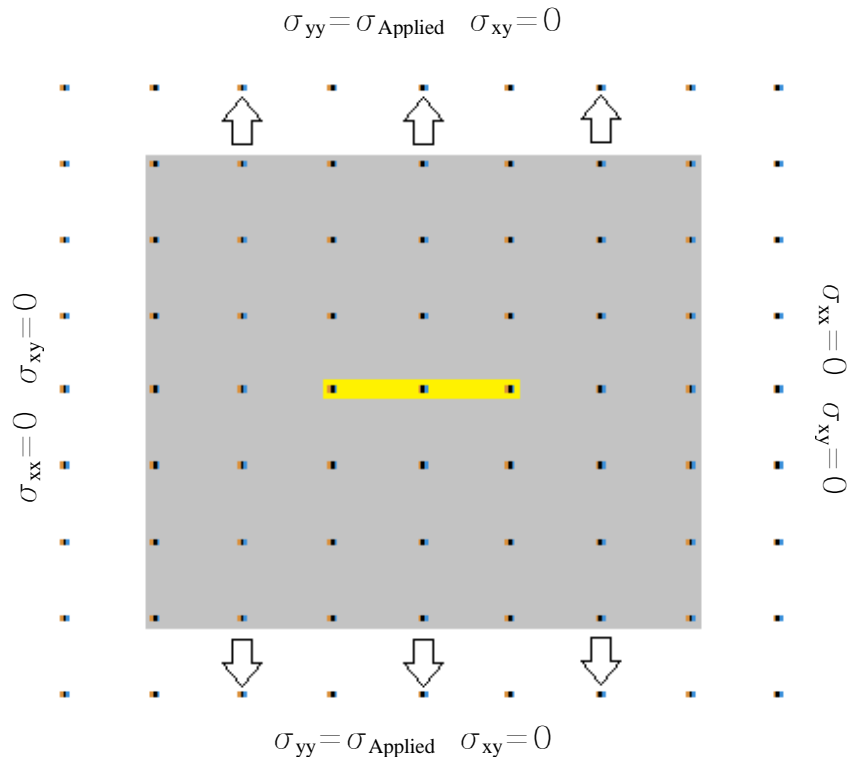


**Figure 8: Tension Test Case Set-up**

From Figure 8, it is clear that this tension test case will have multiple lines of symmetry. These lines of symmetry can be seen in Figure 9.

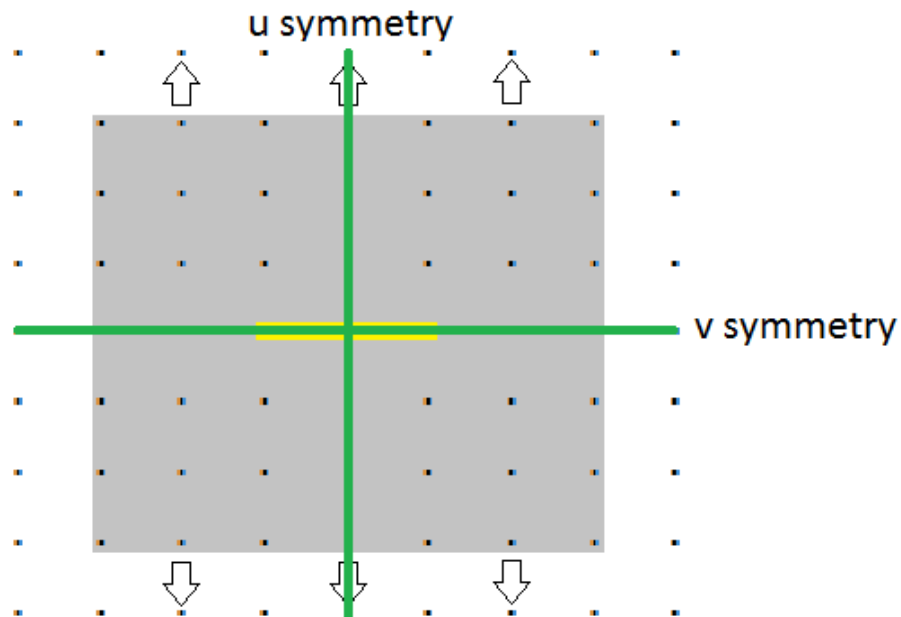


**Figure 9: Tension Test Case Symmetry**

As you can see with this test case the results should all be symmetric about the lines shown. Along the lines of symmetry the displacement is zero as well. This means that only a quarter of the plate needs to be modeled. By modeling just a quarter of the plate, it was possible to increase the resolution of the mesh by four times without any additional computational cost. For example, instead of the entire plate being 200x200, we can make just the quarter of the plate 200x200, therefore making the entire plate 400x400. This increased resolution leads to better more reliable results. Figure 10 shows the boundary conditions that were used to model the quarter of the plate.

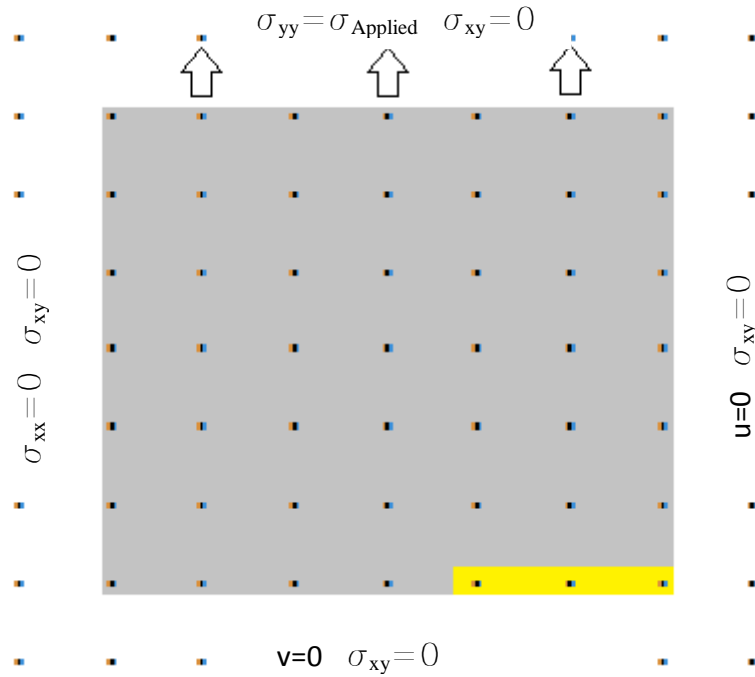


**Figure 10: Symmetry Boundary Conditions**

As seen in Figure 10, the shear stress is set to zero on all four sides of the plate. Next, a normal stress was applied to the top section, and the left side was set to traction free boundary conditions. Finally the symmetry boundary conditions were applied as shown. These symmetry boundary conditions fix the vertical displacement along the bottom edge and the horizontal displacement along the right edge.

After a tension test case run, all of the results were mirrored about the two different lines of symmetry using special post processing functions to produce results comparable to a plate with a crack in the center.

## Finite Difference Code

### Finite Difference Formulation

The finite difference method is a numerical way to approximate the solution to differential equations. This is done by using finite difference equations to approximate derivatives. These approximations are shown in equations (22-24)<sup>[14]</sup>. The index  $i$  represents the “x” direction and the index  $j$  represents the “y” direction.

$$\text{First order:} \quad \frac{du}{dx} = \frac{u_{i+1,j} - u_{i-1,j}}{2\Delta x} \quad (22)$$

$$\text{Second order:} \quad \frac{d^2u}{dx^2} = \frac{u_{i+1,j} - 2u_{i,j} + u_{i-1,j}}{\Delta x^2} \quad (23)$$

$$\text{Second order mixed:} \quad \frac{d^2u}{dx dy} = \frac{u_{j+1,i+1} - u_{j+1,i-1} - u_{j-1,i+1} + u_{j-1,i-1}}{4\Delta x \Delta y} \quad (24)$$

These approximations are substituted into the governing differential equations. In this case, they were used in all of the various differential equations, mostly representing stress equilibrium, applied stresses, or displacements of the nodes. A more in depth discussion of how finite difference works can be found in Richard Haberman’s book, Applied Partial Differential Equations with Fourier Series and Boundary Value Problems<sup>[15]</sup>.

At each node the horizontal and vertical displacements,  $u$  and  $v$  respectively, were the unknowns. Two equations were created at each node using the finite difference approximations in conjunction with boundary conditions or stress equilibrium equations. This results in two equations and two unknowns for each node, which allows for the unknown displacements to be solved using a linear simultaneous equation solver.

## Sections of Equations

### Interior Equations

The interior section of the plate uses stress equilibrium equations. This section is shown in Figure 11.

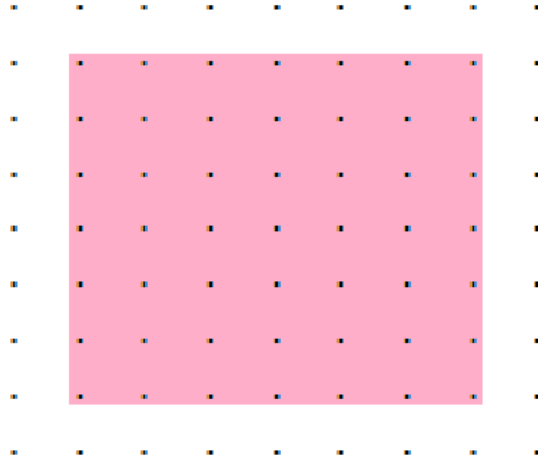


**Figure 11: Interior Nodes**

The equilibrium equations (25 and 26) are:

$$\sigma_{xx,x} + \sigma_{xy,y} = 0 \quad (25)$$

$$\sigma_{yy,y} + \sigma_{xy,x} = 0 \quad (26)$$

The equations for the stresses can be written in terms of material constants and strains. Through the finite difference approximations, these strains can be written in terms nodal displacements. This results in equations which can be used to solve the displacements in terms of the current phase indicator,  $\phi$ . The stress equations are modified to include the phase of the material as discussed in the theory section.



## Sides

The side  $n+1$  nodes, as shown in the Figure 12, contain all of the information regarding the boundary conditions.

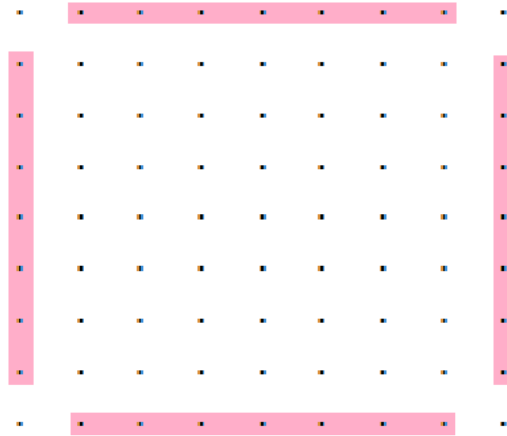


**Figure 12: Side nodes**

The boundary conditions contained in these nodes are either stress or displacement boundary conditions. Remember, these side nodes are “ $n+1$ ” nodes. The displacement at these nodes is not important. Rather, the equations that they represent are used to specify the stress boundary conditions at the edge of the material.

## Corners

The corners are the last section of equations to be specified. The corners are seen in Figure 13.

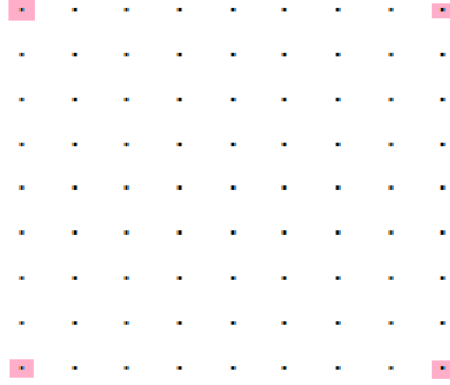


**Figure 13: Corner Nodes**

The corners proved to be difficult. At this point, all of the interior equations have been applied, as well as the boundary conditions at each point. Additional constraints were needed for the corners. It was decided that a second order Taylor Series would be used to predict the displacement at the corners. To do this, a normal second order Taylor Series was written out as seen in equation (27).

$$f(x + dx) = f(x) + \frac{df}{dx}(dx) + \frac{d^2f}{2*dx^2}(2dx)^2 \quad (27)$$

The finite difference approximations were then plugged into the Taylor Series, and expanded about the  $u_{i-1}$  term producing equation (28).

$$u_{i+1} = u_{i-1} + \frac{u_i - u_{i-2}}{2dx} 2dx + \frac{u_i - 2u_{i-1} + u_{i-2}}{2dx^2} (4dx)^2 \quad (28)$$

This then simplified into equation (29).

$$-u_{i+1} + 3 * u_i - 3 * u_{i-1} + u_{i-2} = 0 \quad (29)$$

This Taylor Series uses the previous three nodes, leading to the corner of the plate, to predict the displacement of the corner. This simplifies to a forward difference approximation for setting the change in the curvature (second

derivative) equal to zero. For the vertical displacement, the three nodes used were ones vertically in line with the corner. Similarly, for the horizontal displacement, the three nodes used were the ones horizontally in line with the corner. This assumption could be made because the corners were far enough away from the crack that the displacement at that point is a near linear function of the position, or a constant strain.

### **Displacement Boundary Conditions**

The last section of boundary conditions to be specified are the displacement boundary conditions. These boundary conditions prevent rigid body translation and rotations. In Figure 14, the red highlighted nodes are where the vertical displacements are fixed for the shear test case. Similarly, the yellow highlighted nodes are where the horizontal displacement is fixed.

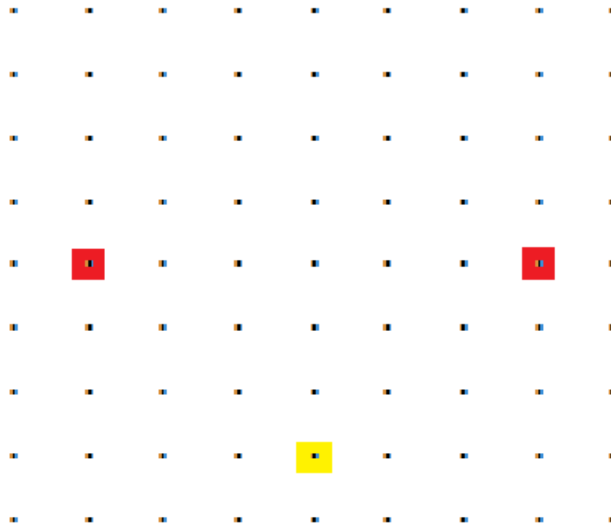


**Figure 14: Displacement Boundary Conditions**

These boundary conditions were chosen due to the fact that they prevent 2-D ridged body translation and rotation without causing any stress concentrations. Explaining how they are implemented is a bit more confusing. The key is that in both test cases, the shear stress is either zero or the applied shear stress the entire way around. This means that the  $n+1$  nodes, 1 away from the corner on both sides of the corner, apply the same equation twice. An illustration of this phenomenon is shown in Figure 15.

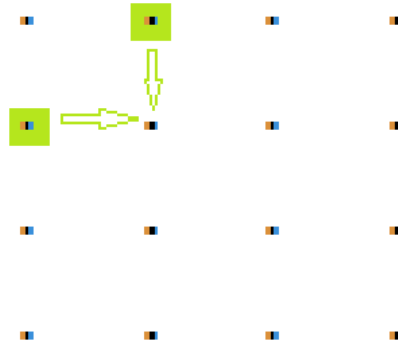


**Figure 15: Location of equations for displacement conditions**

As seen in the green highlighted nodes, both of these  $n+1$  nodes apply the same condition to the same node resulting in four repeated equations. In order to have enough equations to apply three displacement boundary conditions, to properly fix the plate, three of the four repeated shear equations are used instead to specify the displacement boundary conditions. The last repeated shear equation used a Taylor Series similar to the corner as its equation.

## Phase Finite Difference Representation

To include the phase in the finite difference code, a forward difference was used for the terms dependence. Initial conditions for the phase of the material is the same for both the shear and tension test cases. For initial conditions, the entire plate is set to virgin material (phase is 1), except where the crack is. Where the crack is the phase is set to .01. These initial conditions are shown in Figure 16:

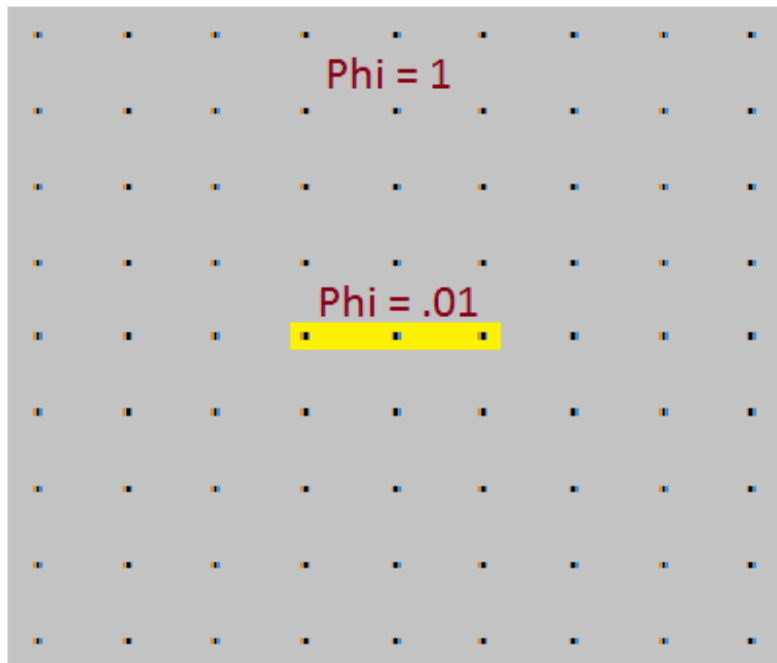


**Figure 16: Phase initial conditions**

Figure 16 shows the initial condition of the shear test case. For the tension test case, the crack is moved to the lower right hand corner due to the symmetrical conditions previously discussed.

As mentioned, in order to allow the phase to diffuse with time a forward difference was used for the time derivative. On every time step the next  $\tilde{v}$  is calculated (recall the phase is a function of  $\tilde{v}$ ) . The forward difference equation uses information from its current state, phase, displacements, and stresses, to determine what the phase should be in the next time step. This equation is used at every node in every time step. The phase boundary conditions were different for both the shear and the tension test cases. In the shear test case, where the crack is initiated, the phase is kept at .01. In this case the edges of the material are kept at phase equal to 1. This is shown in the Figure 17:

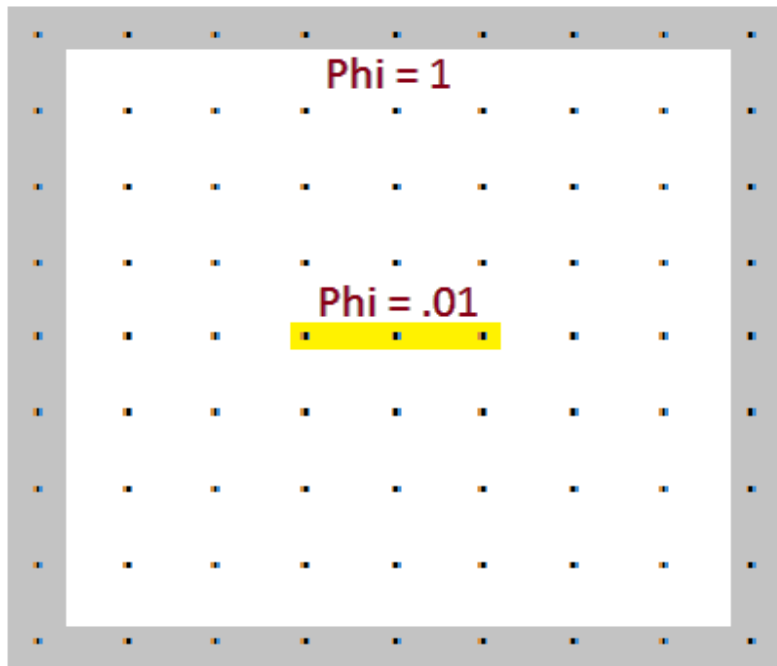


**Figure 17: Shear Test Case Phase B.C.**

Due to the symmetry involved in the tension test case, the phase boundary conditions are more complicated. Similar to the shear test case, on the left and top edges, the phase was kept at 1; also the phase was kept at .01 where the crack

was initiated. Due to the symmetry involved in this case, on the right and bottom edges, symmetry boundary conditions were used. On the right edge  $d\phi/dx$  was set to zero. Similarly on the bottom edge  $d\phi/dy$  was set to zero. These boundary conditions are shown in Figure 18:

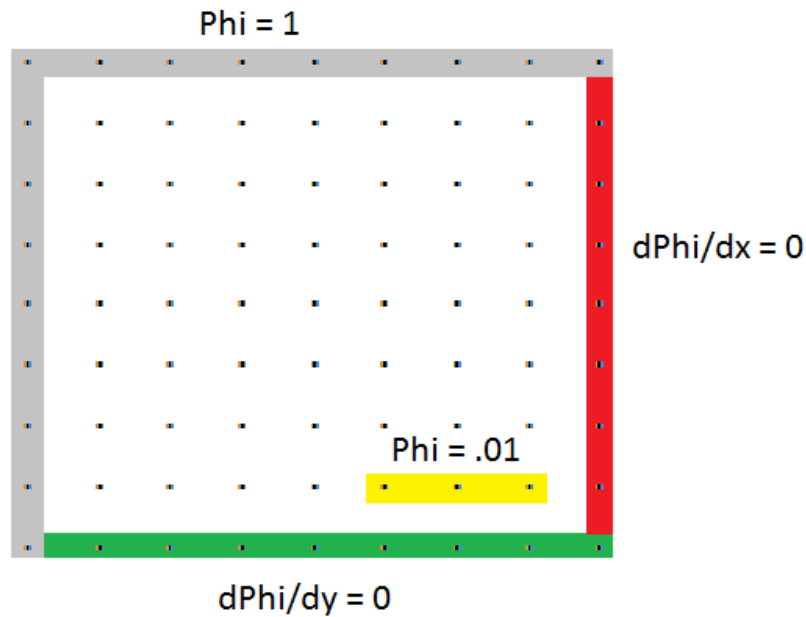


**Figure 18: Tension test case phase B.C.**

In Figure 18, remember that the outer ring of nodes is the  $n+1$  nodes. This is why the crack does not continue to the edge of the plate.

A failed material figure was created to show the propagation of the crack as seen in the results section. This figure was created by using a separate matrix that was the same size as the plate. Initially each node was set to the total number of time steps. As the plate was run through the time steps, when the phase fell below .5, the node was considered to be failed. When this occurs the node that fell below .5 is now assigned a value of the current time step. By the time the

code is finished, a matrix is created that has the time step that each node failed at, or if it didn't fail, it reads the final time step. A contour plot of this matrix is easy to make with the Matlab at this point.

### **Building the Matrix**

The bulk of the finite difference code written is to build the “stiffness matrix”. While this matrix is not necessarily a direct stiffness matrix that is created during a finite element analysis, it is easiest to visualize it as one. As previously stated, there are two unknowns that are solved for at each node, the vertical and horizontal displacement. This means that there needs to be twice as many equations as there are nodes in each plate. So for a 200x200 plate, there are 40,000 nodes. Each node has two unknowns so 80,000 equations need to be created. As discussed above, the equations can be broken down into sections. Using matrix algebra, the governing equation (30) is created:

$$[\textit{Left Hand Side}] = [\textit{Stiffness Matrix}] * [\textit{Unknown Displacements}] \quad (30)$$

In equation 30 the left hand side is created to store the result of each independent equation. The left hand side matrix is a 1 column matrix that has two rows for each node. For this project the left hand side is very sparse, the only non-zero values are where loads are applied. The unknown displacements matrix is a 1 column matrix that represents the horizontal and vertical displacements of each node. Its composition is shown below:



$$\begin{bmatrix} u_{1,1} \\ u_{1,2} \\ u_{1,3} \\ \vdots \\ u_{j+1,i+1} \\ v_{1,1} \\ v_{1,2} \\ v_{1,3} \\ \vdots \\ v_{j+1,i+1} \end{bmatrix}$$

As stated before, the stiffness matrix was the hardest to create. Creating it became a book keeping problem. Each row of the matrix is an independent linear equation. Each row contains one coefficient that lines up with an unknown displacement. This is shown in the matrix below:

$$\begin{bmatrix} U_{1,1} & U_{1,2} & U_{1,3} & \cdots & U_{j+1,i+1} & V_{1,1} & V_{1,2} & V_{1,3} & \cdots & V_{j+1,i+1} \\ \vdots & \vdots & \vdots & \vdots & \vdots & \vdots & \vdots & \vdots & \vdots & \vdots \\ U_{1,1} & U_{1,2} & U_{1,3} & \cdots & U_{j+1,i+1} & V_{1,1} & V_{1,2} & V_{1,3} & \cdots & V_{j+1,i+1} \end{bmatrix}$$

After creating this set up, each row needs to be filled in with at least one non-zero number. As previously stated, each node has two unknowns and two equations. Using equations (31) and (32) the rows for each node with position  $i$  and  $j$  can be found.

$$Row\ 1 = (j - 1) * \left( \frac{length_x}{dx} + 3 \right) + i \quad (31)$$

$$Row\ 2 = (j - 1) * \left( \frac{length_x}{dx} + 3 \right) + i + \left( \frac{length_x}{dx} + 3 \right) * \left( \frac{length_y}{dy} + 3 \right) \quad (32)$$

For example, on a 200x200 plate, let's say that we need to apply two equations to an interior node at  $i = 50$  and  $j = 100$ . This means that we would use rows 20,147 and 61,356 of the stiffness matrix to apply the equations.

Not only do these equations point to rows to be used, but they can also be used to find the correct column to be used. For example, if want to know the column location where  $i = 50$  and  $j = 100$  is located we can use the same equations. The row 1 equation will point to the column of the  $u$  displacement coefficient and the row 2 equation will point to the column of the  $v$  displacement coefficient.

### **Solving the Matrix**

As per equation (30) we have  $[LHS] = [Stiffness\ matrix] * [unknown\ displacements]$ . This equation can be directly solved in Matlab using a sparse matrix solver, and can be formally written as seen in equation (33).

$$[Unknown\ Displacements] = [Stiffness\ Matrix]^{-1} * [LHS] \quad (33)$$

Matlab was used to solve the simultaneous equations for the unknown displacements. The solution vector contains the displacements of each of the nodes.

### **Applying Equations**

There were three types of equations that needed to be applied and inserted into the stiffness matrix. They are displacement, Taylor series, and stress equations. Each is discussed below in more detail.

### **Displacement**

Applying a displacement equation is straight forward. For example let's say that we want to apply a boundary condition and fix the bottom center  $v$ . In our 200x200 plate for example, we first use equation (31 or 32) for  $i = 101$ , and  $j$

= 1. We find that we can use either row 101 or row 41,310 (the choice of the row is not critical). Remember that the first row on the plate is an  $n+1$  row, meaning that it is off the plate. This means that we need to apply the condition to the row above, in order to fix the bottom center of the plate. Since we want to fix  $v$  at that node, the vertical displacement, we will use the row 2 equation, with  $i = 101$  and  $j = 2$ , to find the column of the node that we want to fix. This results in column 41,513. So we now go to row 41,310 and column 41,513 and set it equal to 1. We then go to the LHS matrix and apply the displacement of that node, 0, to the same row that we applied the equation to.

### Taylor Series

Applying the Taylor series equations for corners is very similar to applying displacement conditions. The previously derived equation (34) is used.

$$-u_{i+1} + 3 * u_i - 3 * u_{i-1} + u_{i-2} = 0 \quad (34)$$

For example, let's say that we want to apply the equation to the upper right corner's horizontal displacement. To start we locate the row corresponding to this location using equation (31). For a 200x200 sized plate we use  $i = 203$  and  $j = 203$  and determine that we can use row 41,209. This location also corresponds to the column of the corners location in the matrix as well. The following 4 terms seen in Table 2 are now applied to the matrix:

Row	Column	Value
41,209	41,209	-1
41,209	41,208	3
41,209	41,207	-3
41,209	41,206	1

**Table 2**

Finally the left hand side matrix is updated. The Taylor Series equation should be set to zero, so the corresponding row, row 41,209, in the left hand side matrix is now set to zero.

## **Stress Equations**

In the stiffness matrix, 3 different types of stress equations are applied. The three types are interior stress equilibrium equations, normal stress boundary conditions, and shear stress boundary conditions.

### **Interior Stress Equilibrium Equations**

As previously discussed, the interior stress equilibrium equations are shown below in equations (35 and 36).

$$\sigma_{xx,x} + \sigma_{xy,y} = 0 \quad (35)$$

$$\sigma_{yy,y} + \sigma_{xy,x} = 0 \quad (36)$$

In order to be implemented in a finite difference code the equations must be expanded into equations in terms of material constants, displacements, and the phase of the material. First using a modified version of Hook's law,<sup>[16]</sup> the definitions of stress are written in terms of strains, material constants, and the phase of the material. The stress-strain relation laws can be seen in equation (38). Next strain-displacement relations, found in equation (37) are substituted into the stress-strain equations. Finally taking the appropriate derivatives, the first stress equilibrium equation can be expanded as shown below in equation (39).

$$\varepsilon_{xx} = \frac{du}{dx} \quad \varepsilon_{yy} = \frac{dv}{dy} \quad \varepsilon_{xy} = \frac{1}{2} \left( \frac{du}{dy} + \frac{dv}{dx} \right) \quad (37)$$

$$\sigma_{xx} = [\lambda(\varepsilon_{xx} + \varepsilon_{yy}) + 2\mu\varepsilon_{xx}]G(\phi) \quad \sigma_{xy} = [2\mu\varepsilon_{xy}]G(\phi) \quad (38)$$

$$\begin{aligned} & \left[ \lambda \left( \frac{d^2u}{dx^2} + \frac{dv}{dx dy} \right) + 2\mu \frac{d^2u}{dx^2} \right] G(\phi) + \left[ \lambda \left( \frac{du}{dx} + \frac{dv}{dy} \right) + 2\mu \frac{du}{dx} \right] G'(\phi) \frac{d\phi}{dx} + \\ & \mu \left[ \frac{d^2u}{dx^2} + \frac{d^2v}{dx dy} \right] G(\phi) + \mu \left[ \frac{du}{dy} + \frac{dv}{dx} \right] G'(\phi) \frac{d\phi}{dy} = 0 \end{aligned} \quad (39)$$

Next, using the finite difference approximations for the differential terms, the differential terms can be expanded to result in a final equation in terms of  $u$ ,  $v$ , material constants  $\mu$  and  $\lambda$ , and  $\phi$ . This equation can now be put into the stiffness matrix as previously discussed at this point. The second stress equilibrium equation can be expanded with the same process. Also the left hand side matrix row corresponding to this equation is zero; so similar to the previous examples, the corresponding row of the left hand side matrix is set to zero.

### Normal Stress Boundary Conditions

The normal stress boundary conditions are applied in the same manner as the stress equilibrium equations. The normal stress in the  $yy$  direction can be written as shown in equation (40).

$$\sigma_{yy} = \sigma_{applied} \text{ or } 0 = [\lambda(\varepsilon_{xx} + \varepsilon_{yy}) + 2\mu\varepsilon_{yy}]G(\phi) \quad (40)$$

The previous strain-displacement equations and finite difference approximations are substituted into the equation, resulting in an equation in terms of  $u$ ,  $v$ , material constants, and the phase of the material. Also the left hand side matrix needs to be updated in the equation to either zero for a traction free surface, or to an applied stress.

### Shear Stress Boundary Conditions

The shear stress boundary conditions are applied in the same manner as the normal stress boundary conditions. The shear stress boundary condition is shown in equation (41).

$$\sigma_{xy} = \sigma_{applied} \text{ or } 0 = 2\mu\epsilon_{xy}G(\phi) \quad (41)$$

The previous strain-displacement equations and finite difference approximations are substituted into the equation, resulting in an equation in terms of  $u$ ,  $v$ , material constants, and the phase of the material. Also the left hand side matrix needs to be updated in the equation to either zero for a free surface, or to an applied stress.

### Variable Time Step

One thing that was done to increase the stability of the code was to include a variable time step. At each time step of the code, the program runs through each point and determines what the required time step is to keep the program stable. The required time step is a function of the maximum stress of any point in the plate. The code then applies this time step to each node for the forward difference phase equation. This modification was successful in increasing the numerical stability of the code.

### Speeding up the Code

There were many things done to improve the performance of the finite difference code. The biggest problem was dealing with the resulting size of the

stiffness matrix that is generated. For example, a 10x10 mesh produces 100 nodes, with each node having two equations and unknowns, resulting in 200 equations and unknowns total. The resulting stiffness matrix is now 200x200, which is easily constructed and solvable, almost instantly. However, a much finer mesh is needed. The goal was to use a 200x200 mesh. This results in 80,000 equations and unknowns. This also means that the stiffness matrix is 80,000x80,000. Constructing and solving this system of equations takes a considerable amount of time, especially when hundreds of time steps are needed.

Two main things were done in order to speed up the computational time. First, the code was modified to be run on a cluster. The code was made to run stand alone, and save its results to data files. By running on the cluster, a run that would take well over 48 hours on a PC could be done in less than 8 hours. Also dozens of runs could be executed at the same time. This proved to be key when tuning the parameters of the model.

Also the computational time was reduced by noticing the matrices are sparse. In a 200x200 mesh, the stiffness matrix generated is more than 99.99% zeros. By generating all of the zeros in the matrix, and then solving the system of equations the standard solvers used proved to be much slower. By using a sparse matrix and a sparse matrix solver, the code was sped up by a factor of 6.

## Program Structure

The actual program for this thesis was created in Matlab. Matlab was chosen as it contains a great deal of convenient built in functions, is very user friendly for working with large matrices, and has excellent plotting functions<sup>[17]</sup>. Two different versions of the code were created, one for each test case. The code section for each case is slightly over 1,000 lines. A flow chart of the code can be seen in Figure 19.

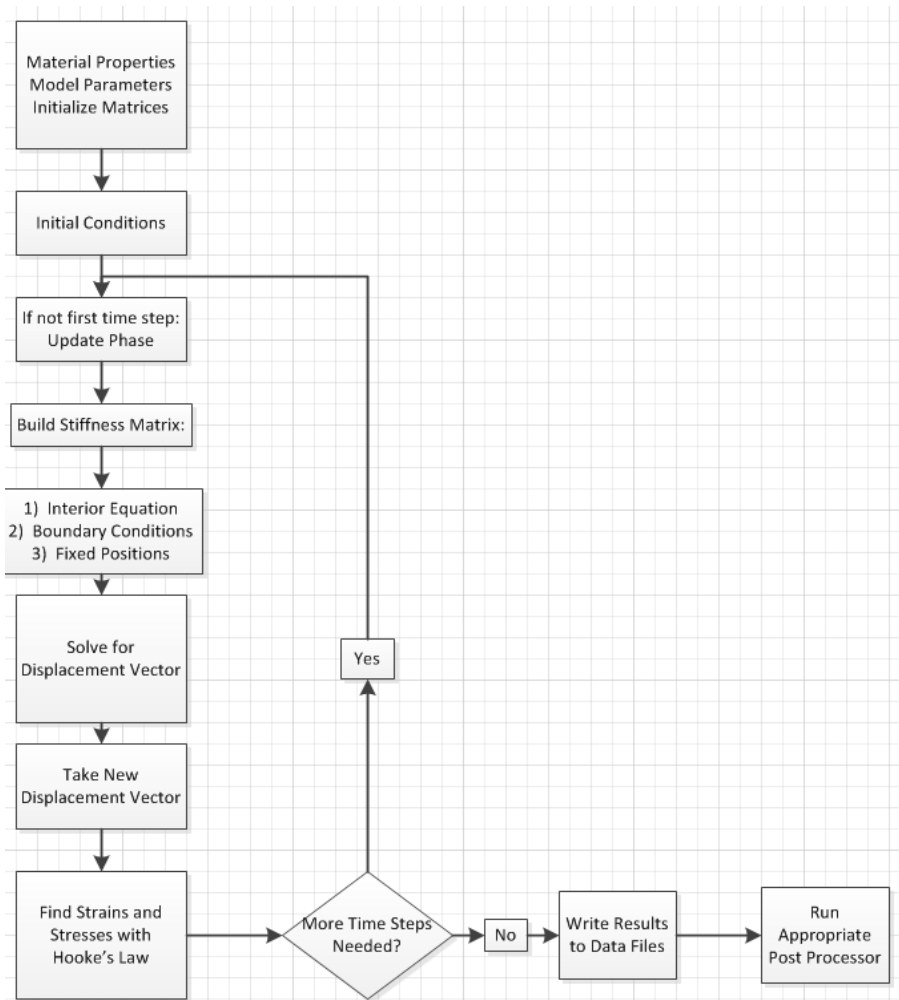


**Figure 19: Program Flow Chart**



The program starts out by specifying the material properties to be used such as  $\mu$  and  $\lambda$ . Next model parameters are specified. This includes items such as the size of the plate, the amount of loading to be applied, or the number of time steps to be run. Next, all of the matrices are initialized for their size only. There are a great number of matrices that are initialized at this point such as the strain, stress, displacement, phase, and many more. Next initial conditions are specified such as phase and displacement initial conditions. Also other matrices that are functions of the phase or displacement, such as  $G(\phi)$ , are specified at this time.

At this point we are into the section of the code looped throughout every time step. This section of the code starts out by updating the phase of the material though the forward difference method previously discussed. This is done every iteration, except the first time when the initial conditions for the phase are used instead. Next, the stiffness matrix is built. This is a very complex process that contains two main sections, the first is for the interior governing equations and the second is for the boundary conditions. The interior section contains two main subsections, one for each governing equation. The stiffness matrix is traversed row by row and the appropriate equation is applied. Next in a similar fashion to how the interior equations were applied by traversing each row, the stress boundary conditions and Taylor series boundary conditions are applied. The last thing that is done is the fixed position boundary conditions are applied. Before continuing the entire matrix is checked to insure that each row contains at least one non-zero constant. Also at this point the matrix is checked to insure that each row in an independent linear equation. These checks helped a great deal for

troubleshooting the code and serve to check that the matrix is not singular. These checks can be disabled after the code is working properly to speed up processing time, but remain useful if cracks propagate to the boundary.

Next the left hand side matrix is created. In this case the only non-zero terms that are present are where loads were applied. Then using the sparse matrix solver in Matlab the displacement vector is found. This displacement vector is then transformed into a displacement matrix that has the same dimensions as the plate. Next the strains are calculated using the strain-displacement laws, and the stresses are found using Hooke's Law.

At this point the code has completed a run though one entire time step. If the code needs to continue to run for more time steps it is looped back up as shown. If not all of the results are written to data files. The files can then be read using a post processor that reads the data files and creates the figures shown in the results section. There are two different post processors that are used. The first is the standard one for the shear test cases. The second is the symmetry post processor that mirrors the results about the lines of symmetry for the tension cases.

## Results

### Shear Results

The first set of results to be discussed is the shear results. In this case, the plate was 200x200 with an initial crack in the center with a length of 40. The shear stress was applied to all four sides. The expectation for this test is that the crack will grow towards the upper left and lower right corners, initially at  $69^{\circ}$ <sup>[18]</sup> and then turning more horizontal as the crack grows. The following results discussed are for a run with 200 time steps.

Figure 20 is the first resulting figure shown and is a contour plot of the final phase of the plate.

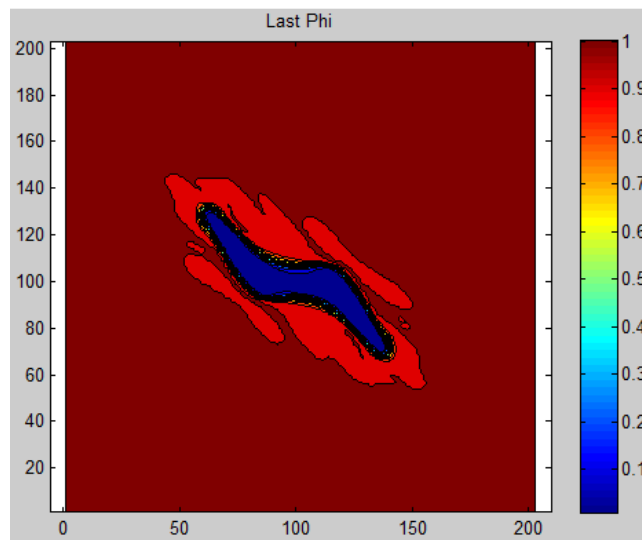
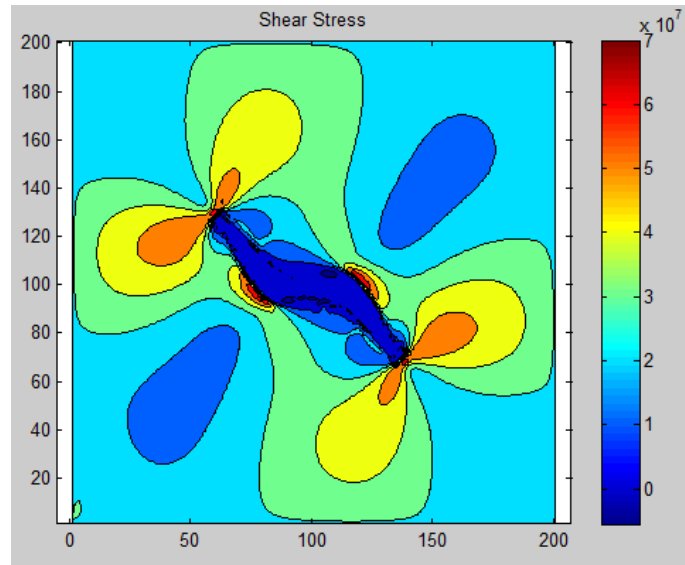


**Figure 20: Final Phase of Plate**

Remember that this crack started out as a single element wide horizontal crack, initiated from 80 to 120 on the x-axis in the middle of the plate. As one can see

the phase is zero where the crack is, and diffuses back to virgin material the further away from the crack you go. It is also important to note how the crack grew towards the upper left and lower right corners.

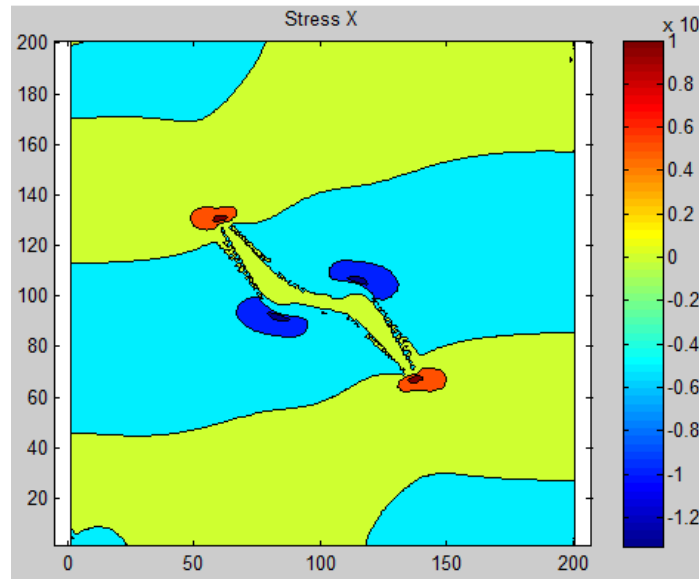
Figure 21 is a contour plot of the shear stress of the plate.



**Figure 21: Final Shear Stress**

Recall in this case the shear loading was constant all the way around. The light blue near the sides show the applied shear. Also, as you can see, where the material has completely failed, the shear stress is nearly zero. This is due to the fact that the modulus of the material is effectively reduced to zero by the modulus modifying function. The next important observation to make are the stress concentrations near the crack tips that are exactly what is expected by fracture mechanic's theory.

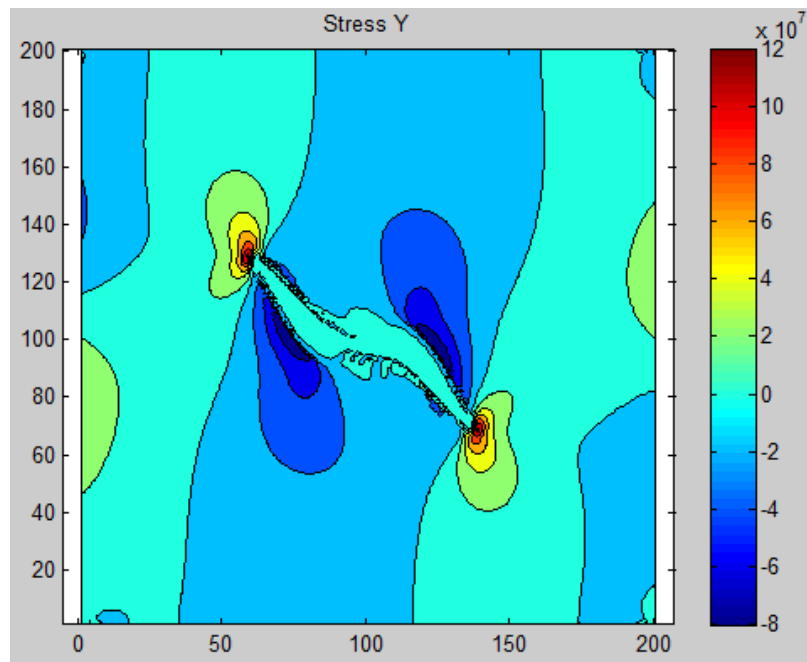
Figure 22 is a contour plot of the stress in the x-direction.



**Figure 22: Stress in the X-Direction**

The stress in the x direction is very small where the material has already failed, as well as far away from the crack. Also worth noting is the tensile stress concentration near the crack tips in the upper left and lower right corners. The upper right and lower left corners have compressive stress concentrations.

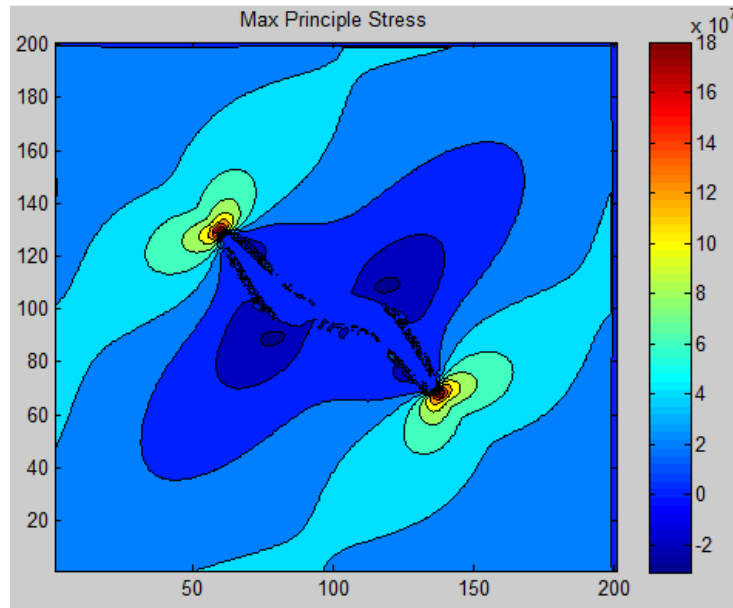
Figure 23 is the stress in the Y-direction.



**Figure 23: Stress in the Y-Direction**

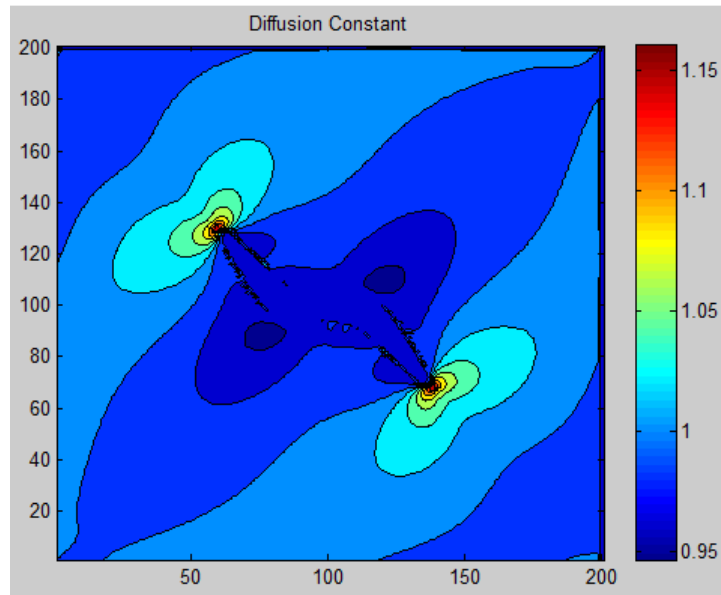
Similar to the stress in the X-Direction, the stress in the Y-direction is low far away from the crack and where the material has already failed. Again, similar to the stress in the x-direction, the tensile stress concentrations are high in the direction of the crack propagation, and compressive in the corners that don't propagate.

Figure 24 shows the maximum principle stress that corresponds to the previous figures.



**Figure 24: Maximum Principle Stress**

As seen in Figure 24, the maximum principle stress occurs on the crack tips. This is expected to happen. One can also see that behind the crack tip the maximum principle stress is very low. This is the key for the variable diffusion constant shown in the next figure. In every stress plot the upper left and lower right contain positive tensile stress concentrations, while the lower left and upper right contain negative compressive stress concentrations. This is what allows the diffusion constant to push the crack in the direction of highest principle stress.



**Figure 25: Diffusion Constant**

In Figure 25 one can really see the power of the variable diffusion constant. The variable diffusion constant allows the crack to diffuse only in the direction of minimum principle stress as previously discussed. Figure 26 and Figure 27 show the direction of the minimum principle stress. This is the direction that the diffusion constant is increased in, driving the diffusion in the direction of the minimum principle stress.



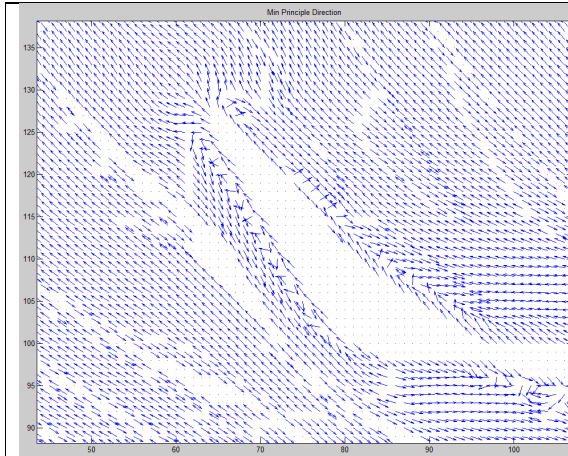


**Figure 26: Left side of Crack, Min Principle Direction**

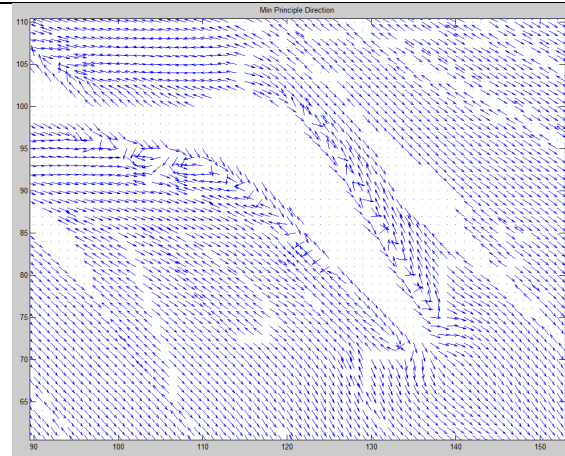


**Figure 27: Right side of Crack, Min Principle Direction**

As one can see the minimum principle direction is pushing the crack towards the upper left and lower right corners. In the other corners of the crack, the principle direction does not push the crack to propagate. Before this term was introduced, the crack would grow toward each of the four corners. This term prevents the growth in the upper right and lower left corners of the crack and encourages the growth to the other corners. Although in the previous figures not all of the arrows point in the precisely exact direction, the overall trend is correct; the crack is only allowed to diffuse in the corners which have positive principle stresses.

Figure 28 plots iso-contour lines on the plate. This can be used to visualize the deformation of the plate. Of course a scaling factor is used here in order to magnify the deformation.

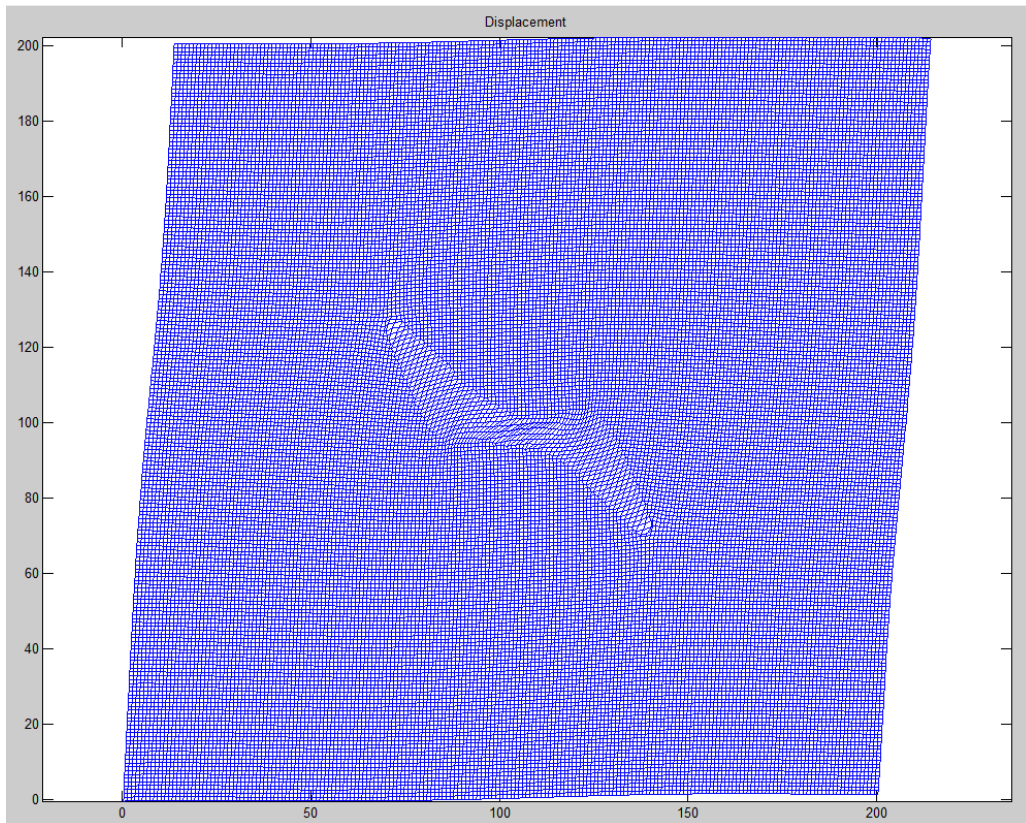


**Figure 28: Deformation of plate**

Figure 28 makes it easy to see the failure of the material where it has cracked.

Essentially the modulus of elasticity is reduced dramatically, which means the material there can be strained a great deal without much stress or resistance.

The final result to be shown is the most exciting. Figure 29 shows how the phase of the material changes with time, essentially showing the cracks propagation.

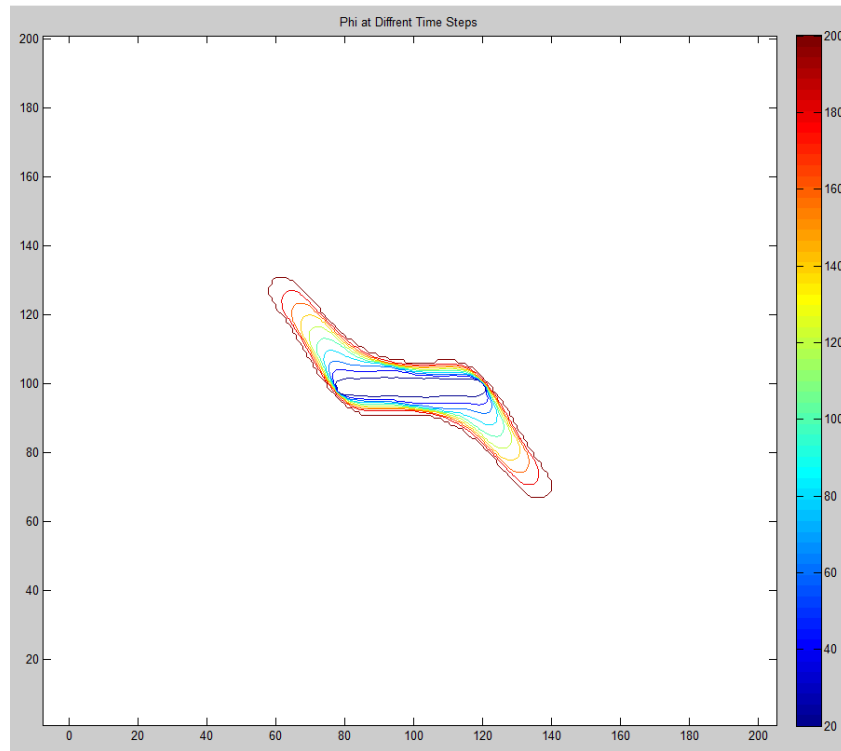


**Figure 29: Phase with time**

Figure 29 shows how the crack diffuses through the material with time. The dark blue lines represent the original location of the crack, while the red lines represent the location of the crack at the final time steps. In order to create Figure 29, it was decided that a phase threshold of .5 was to be used. This means that the material was considered to be failed when the phase fell below .5. It is important to note the crack initially grew at  $69^\circ$ , which is what is predicted by fracture mechanics<sup>[8]</sup>. The crack the curved more horizontal as it grew, which again, this result is supported by fracture mechanics.

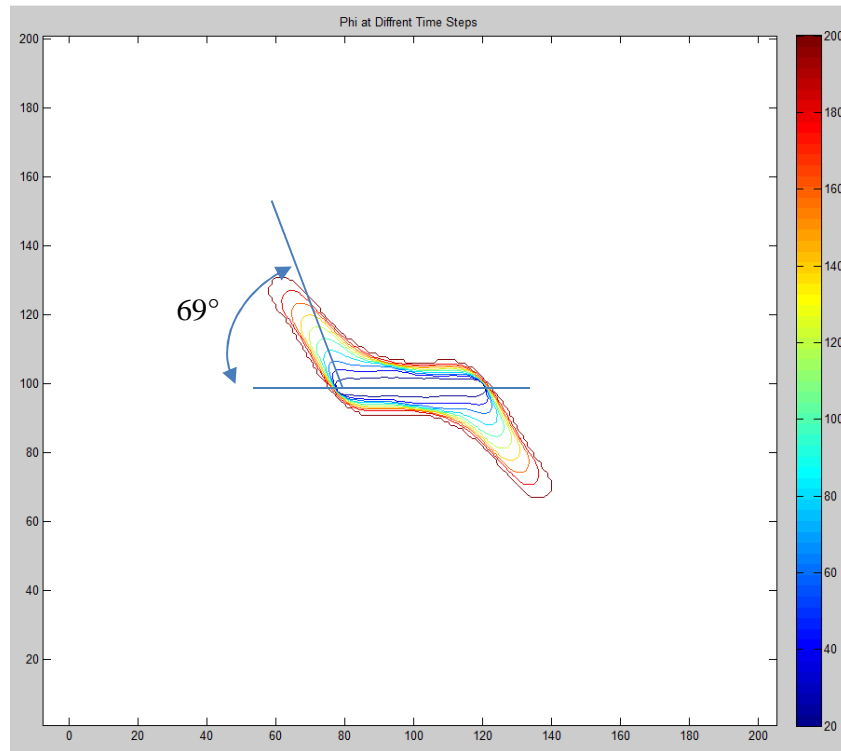


**Figure 30: Measured Kink Angle**

In Figure 30, the phase-time figure was overlaid with a sketch of the predicted initial kink angle. As you can see, initially the crack grew at almost exactly  $69^\circ$  and then curved to become more horizontal. This is exactly what is predicted by fracture mechanics.

Figure 31 shows a run with the same set up before, but run for much longer. In this run the simulation was allowed to run for 400 time steps instead of 200.

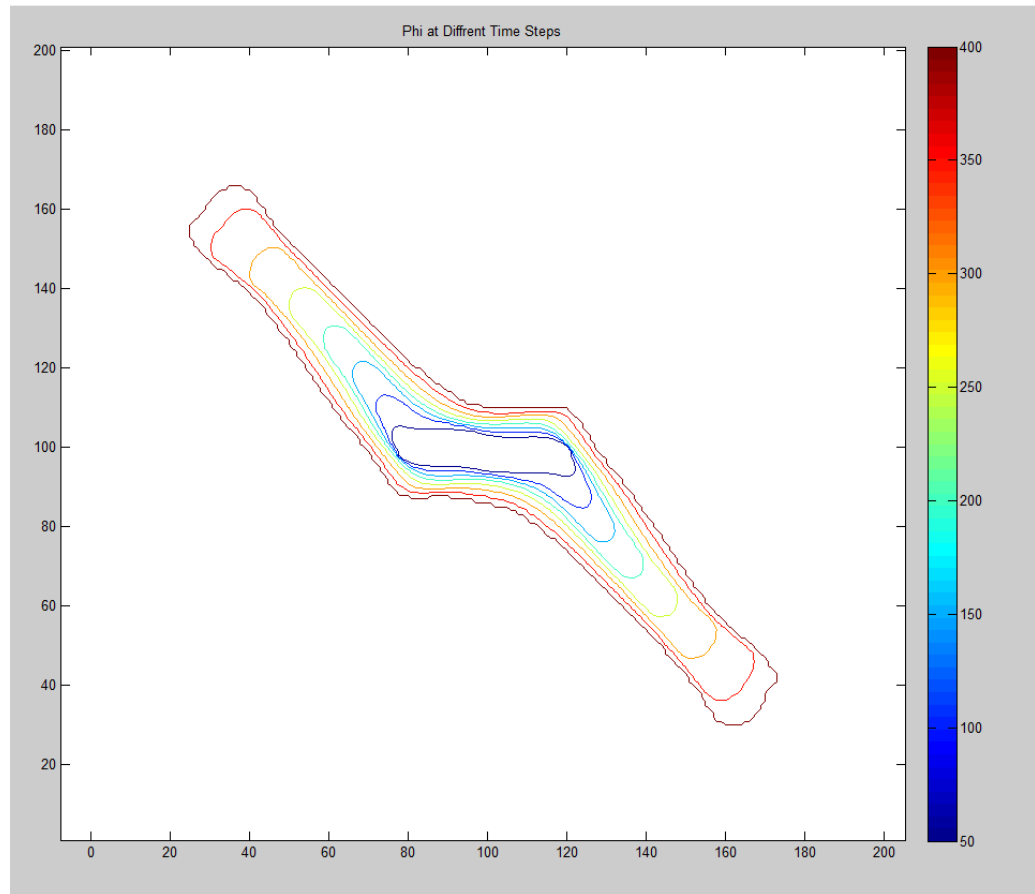


**Figure 31: Doubled Run Time Crack Growth**

As you can see, in this case the crack continued to diffuse as expected. Also in Figure 31 you can see the crack begin to curve to become more horizontal. This is what is expected from fracture mechanics. This figure also shows that the crack settles at a propagation of a constant  $45^\circ$  which is supported by fracture mechanics theory. In addition, at the crack tips, the crack looks as though it is about to bifurcate into two cracks. Compared to Karma's results, which curve to become more vertical, these results are more realistic. However, due to size restraints, the crack takes up the majority of the plate and the sides of the plate are definitely impacting the results. Ideally a much larger plate should be modeled,

however due to the size constraints of the finite difference model it is not computationally possible at this point.

### Tension Results

The next set of results to be discussed is the tension test results. In this case, the plate was 200x200 with an initial crack in the lower right with a length of 40. A normal stress was applied to the top of the plate. Due to symmetry the bottom of the plate was fixed. The results were then mirrored about the lines of symmetry to create the plots seen. This set up is discussed in detail previously in this thesis. The expectation for this test is that the crack will grow straight outwards. The following results shown are the result of a run with 200 time steps.

Figure 32 is the first result shown for the tension test case and is a contour plot of the final phase of the plate.

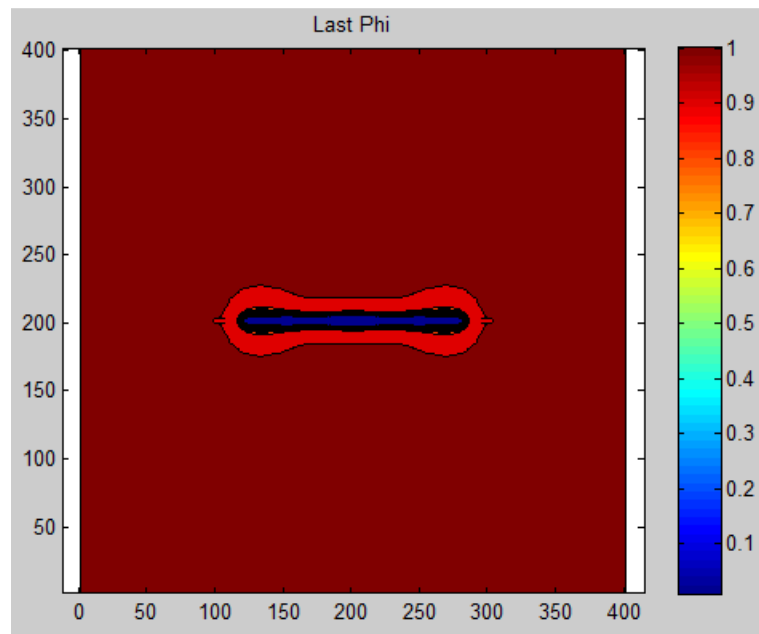


**Figure 32: Final phase**

Remember that this crack started out as a single element wide crack, going from 160 to 240 on the x-axis in the middle. As one can see the phase is zero where the crack is, and diffuses back to virgin material the further away from the crack you go. It is also important to note that the crack grew straight towards the sides of the plate. Also note that the diffusion was predominantly in the direction of the crack growth, with very little vertical diffusion.

Figure 33 is a contour plot of the shear stress of the plate.

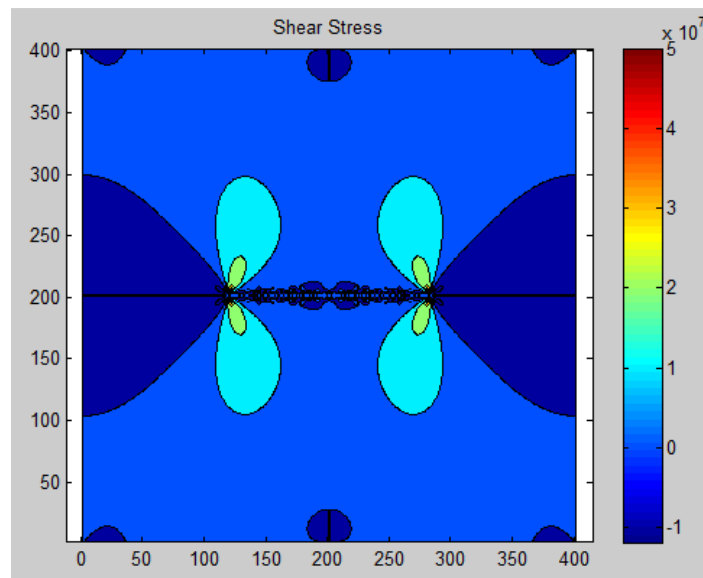


**Figure 33: Final shear stress plot**

As you can see, where the material has completely failed, the shear stress is nearly zero. It is also important to note the correct stress concentrations at the crack tip.

Figure 34 shown is a contour plot of the stress in the x-direction.

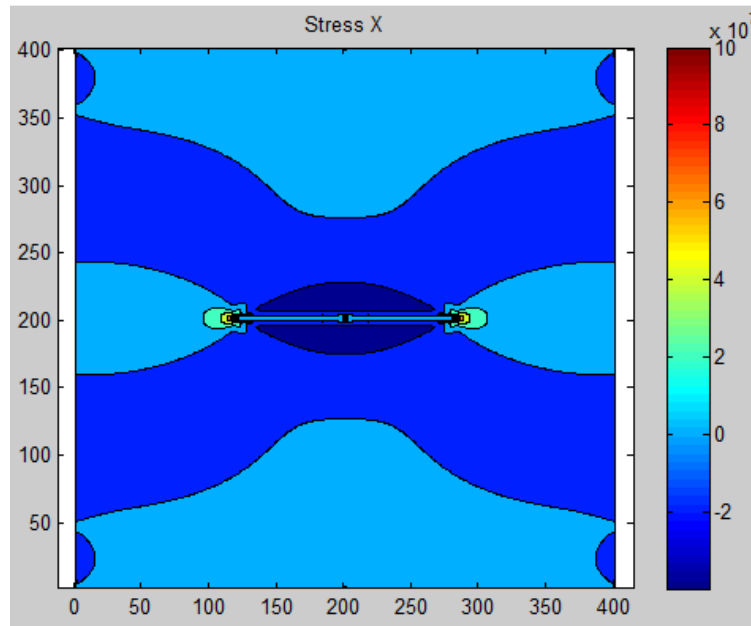
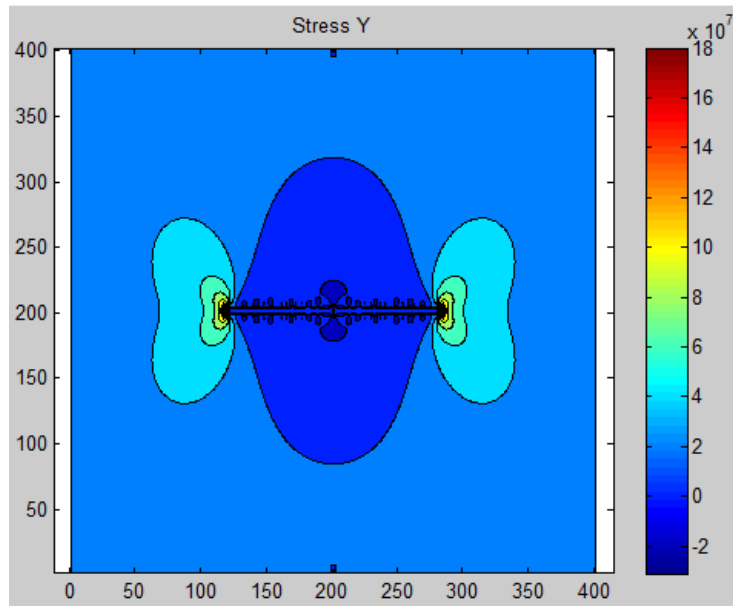


**Figure 34: Final stress-x**

The stress in the x direction is very small where the material has already failed, as well as far away from the crack. The stress concentrations at the tip of the crack are a result of Poissons effect as the plate wants to compress there.

Figure 35 is the stress in the Y-direction.

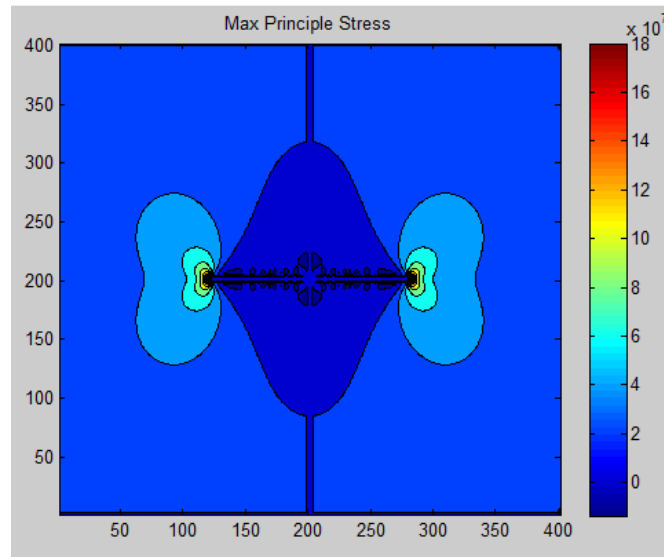




**Figure 35: Stress-y**

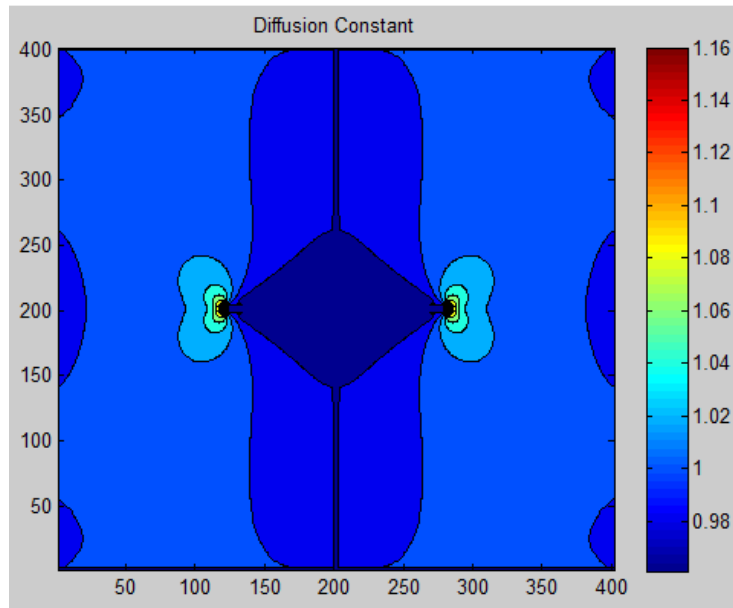
This figure is the most convincing that the model is working correctly for this test case. As one can see, above and below the crack the stress is very small as the material cannot support a load there. At the tip of the crack on both sides there are stress concentrations that are the result of the inner portion of the plate not being able to effectively carry the load. Far away from the crack the stress is constant and equal to the applied stress as expected.

Figure 36 shows the maximum principle stress that corresponds to the previous figures.



**Figure 36: Maximum Principle Stress**

As seen in Figure 36, the maximum principle stress occurs on the crack tips. This is exactly what is expected to happen. One can also see that behind the crack tip the maximum principle stress is very low. This is the key for the variable diffusion constant shown in Figure 37.



**Figure 37: Diffusion Constant**

Similar to the previous test case, in Figure 37 one can really see the power of the variable diffusion constant. The variable diffusion constant allows the crack to diffuse only in the direction of minimum principle stress as previously discussed. Figure 38 and Figure 39 show the direction of the minimum principle stress. This is the direction that the diffusion constant is increased, driving the diffusion in the direction of the minimum principle stress.

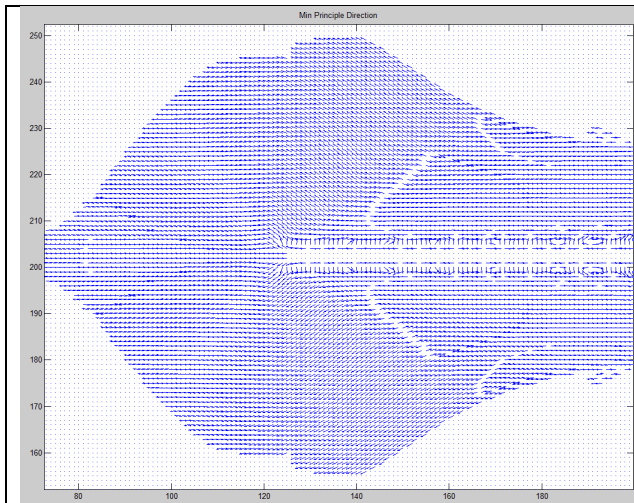


**Figure 38: Left side of Crack, Min Principle Direction**

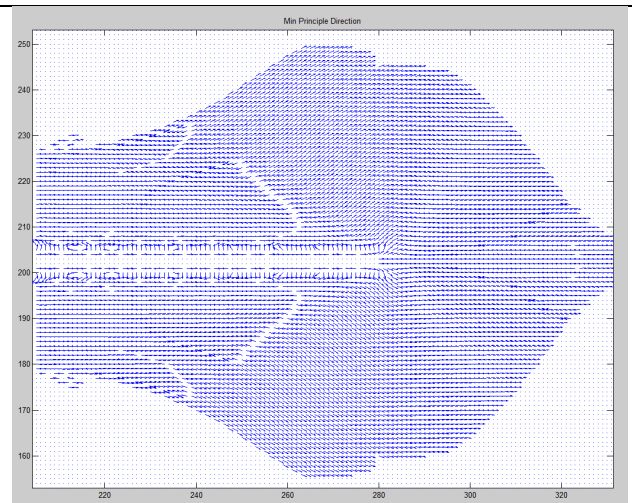


**Figure 39: Right Side of Crack, Min Principle Direction**

As you can see the minimum principle direction is pushing the crack horizontally to the sides of the plate. Although in the previous figures not all of the arrows point in the precisely exact direction, the overall trend is correct.

Figure 40 plots iso-contour lines on the plate. This can be used to visualize the deformation of the plate. Of course a scaling factor is used here in order to magnify the deformation to make it easier to see.

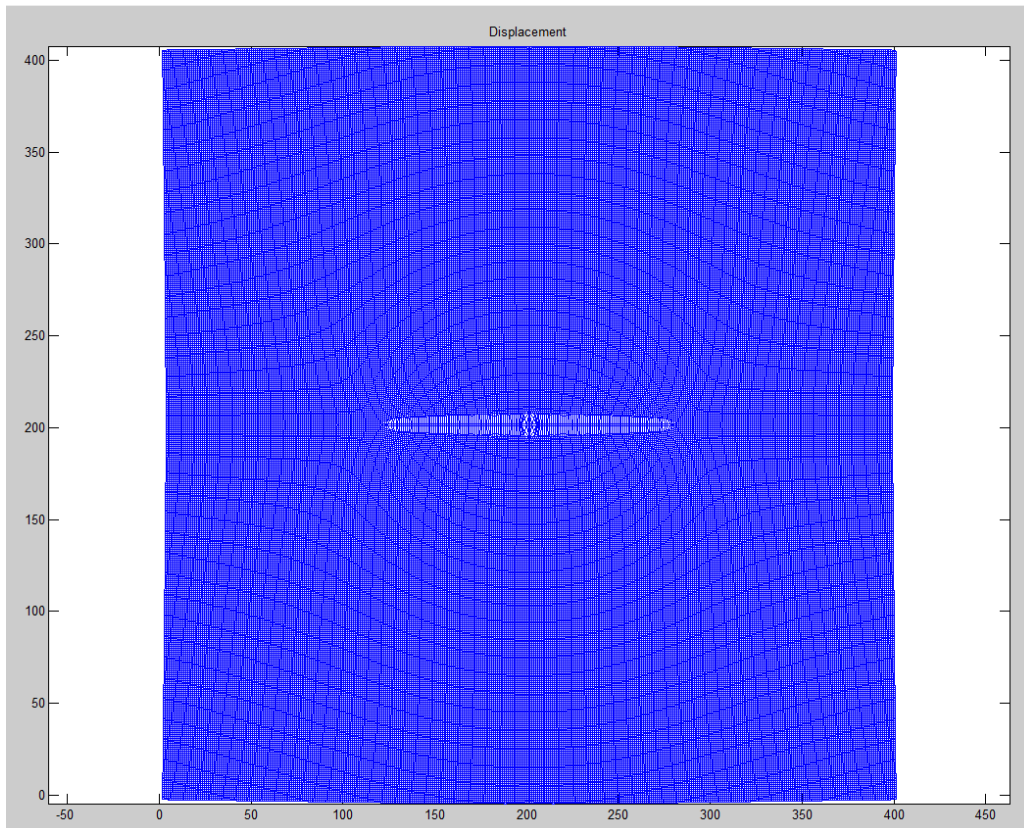


**Figure 40: Deformation**

This deformation figure makes it easy to see where the material has failed.

Essentially the modulus of elasticity is reduced dramatically, which means the material there can be strained a great deal without much stress. Notice that where the crack is the strain is very high. This crack also shows the effect of Poisson's effect with dealing with a crack. This deformation plot also makes it easier to confirm that the stress plots are correct.

The final result to be shown is the most exciting. Figure 41 shows how the phase of the material changes with time.

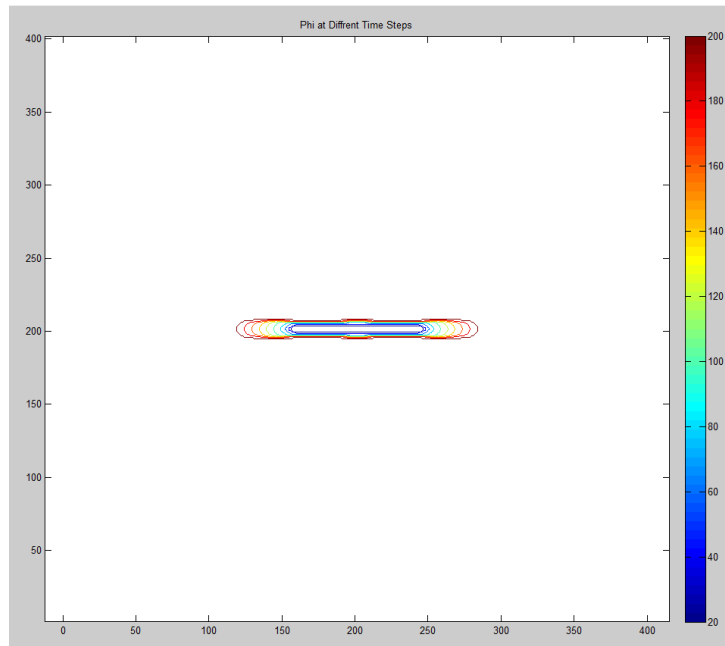


**Figure 41: Phase as a function of time**

This figure shows how the crack diffuses through the material with time. The dark blue lines represent the original location of the crack, while the red lines represent the location of the crack at the final time steps. In order to create this figure, it was decided that a phase threshold of .5 was to be used. This means that the material was considered to be failed when the phase fell below .5. It is important to note the crack grew perfectly horizontal which is what is predicted by fracture mechanics.

### **Stress Intensity Factor**

After creating a model that could accurately model the stress and changes in the phase of the material, the stress intensity factor was found and compared according to fracture mechanics. The stress intensity factor is used when calculating the stress around a crack tip. The tension test case was used when

finding and comparing the stress intensity factor as fracture mechanics solutions exist for the exact problem. According to fracture mechanics, the stress intensity factor,  $K$ , should follow the relationship described in equation (42)<sup>[19]</sup>:

$$K = \sqrt{\pi a} \sigma \quad (42)$$

In this relationship,  $a$  is the radius from the crack tip to the center of the crack. This stress intensity factor was calculated using fracture mechanics as well as from the results of the simulation, and the resulting stress intensity factors were compared. Before comparing the stress intensity factors from the model, a boundary correction factor was calculated<sup>[20]</sup>. The stress intensity factor now assumes the following form as seen in equation (43).

$$K = \sqrt{\pi a} \sigma * F(\alpha, \beta) \quad (43)$$

The function  $F(\alpha, \beta)$  is a modifying function that is a function of the geometry of the plate. With the geometry that is being used  $\alpha$  is equal to the crack length divided by the plate width, or 80/400 which is 0.2.  $\beta$  is equal to the height of the plate divided by the width of the plate. Since we have a square plate,  $\beta$  is equal to 1. From table 1,  $F(0.2, 1)$  was determined to be 1.055<sup>[20]</sup>.

Using a tension test run, the stress intensity factor was found at various times throughout the run. Figure 42 shows one of these calculations.

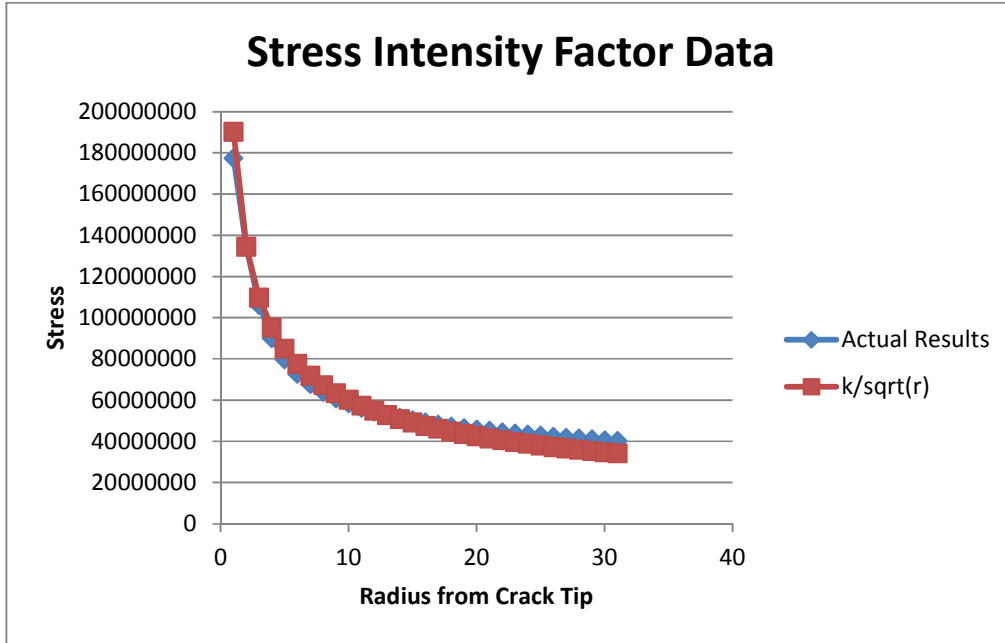


**Figure 42: Stress Intensity Factor Data**

To create this chart, first the actual stress in the yy direction was plotted going away from the crack tip. Next, another function,  $k/\sqrt{\pi \cdot r}$  was created. The error between the two curves was minimized using the solver in excel. This K is then considered to be the stress intensity factor for the case. As you can see from the previous chart the actual results fit the  $1/\sqrt{r}$  shape of the curve quite nicely.

Next the stress intensity factor was calculated using fracture mechanics. Using equation (44) from Rooke for an infinitely long plate a stress intensity factor was calculated<sup>[19]</sup>:

$$K = \sigma * \sqrt{\pi a} \left[ \frac{1 - \frac{a}{W} + .326 * \left( \frac{2a}{W} \right)^2}{\sqrt{1 - \frac{2a}{W}}} \right] \quad (44)$$



In this equation,  $a$  is half of the cracks total length, or the radius to the crack tip from the center of the plate, and  $W$  is the total width of the plate. This stress intensity factor was then compared to the one found from the data for different crack lengths. The result of this comparison can be seen in Figure 43.

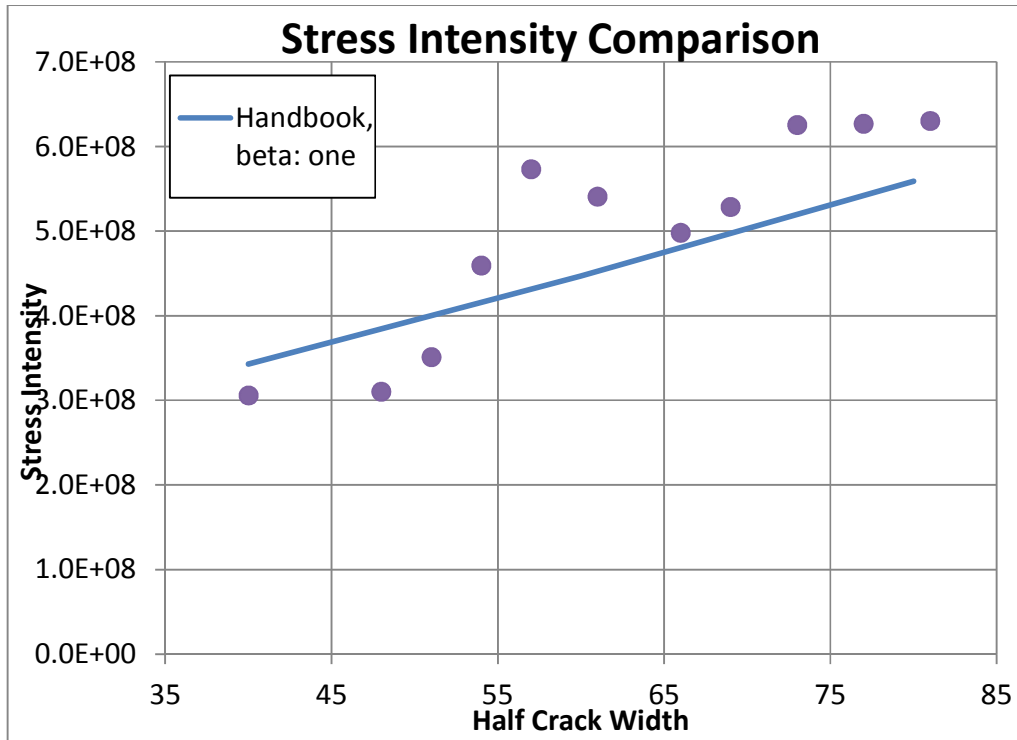


**Figure 43: Stress Intensity Comparison**

Figure 43 shows the final results of the stress intensity comparison calculation. From the figure it is clear that the finite difference solution appears close but not exact. The overall trend is represented fairly closely. However, there is quite a bit of scatter. This scatter can be attributed to various causes. First, the resolution of the crack tip is not fine enough. Most of the stress concentration is within just 15 nodes. Ideally with more nodes near the crack tip, the results would be better. In addition, some of the error can be attributed to the effects of the ends of the

plate. Also to get a better fit for the slope of the experimental results, a better function relating  $\phi$  to  $\tilde{v}$  should be used.

## **Conclusions and Future Work**

From the results of this work it is clear that the phase field physics theory can be appropriately applied to cracks. This theory allows crack propagation to be modeled with great accuracy and increased numerical stability. The phase is shown to diffuse correctly and the corresponding modification to the modulus works as well. The stresses surrounding the cracks are also the expected results that align with the expectations from fracture mechanics as discussed.

The next step is to implement this theory into a finite element code. A custom user element needs to be constructed that will contain the phase of the material as an additional state variable.

## Appendix

### Phase Field Lagrangian Summary

The Lagrangian density can be defined as:

$$\mathcal{L} = \frac{1}{2} \rho \dot{u}_i \dot{u}_i + \frac{1}{2} \rho \dot{\tilde{u}}^2 + \frac{1}{2} \rho \dot{\tilde{v}}^2 - \int^\varepsilon \sigma_{ij}(\tilde{v}, \tilde{u}, \varepsilon') d\varepsilon'_{ij} - V_{DW}(\phi) - u_i F_i - \frac{1}{2} \tilde{K} \tilde{u}_{,i} \tilde{u}_{,i} - \frac{1}{2} \tilde{J} \tilde{v}_{,i} \tilde{v}_{,i}$$

.

Variables and parameters are related through:

$$\tilde{u} = \frac{\dot{\tilde{u}}}{\Omega_0}, \tilde{v} = \frac{\dot{\tilde{v}}}{\Omega_1}, T = \frac{\dot{\tilde{u}}^2}{4c_p}, \phi = \frac{\dot{\tilde{v}}^2}{4(\tau/\rho)}, K' = \frac{\Omega_0 K}{4c_p}, J' = \frac{\Omega_1 D_\phi}{4(\tau/\rho)},$$

$$\sigma_{ij} = C_{ijkl}^0 g(\phi) [\varepsilon_{kl} - \alpha_{kl}(T)(T - T_R) - \varepsilon_{kl}^p].$$

The functions are:

$$g(\phi) = 1 - \frac{(1-\phi)^{m+1}}{n} [(m+n+1) - (m+1)(1+\phi)^n]$$

$$V_{DW}(\phi) = V_0 (1-\phi)^2 (1 + 2\phi + \alpha\phi^2)$$

The remaining parameters can be temperature,  $T$ , dependent. Note that we can take  $K' = G$  for isotropic and cubic materials and hence  $\Omega_0 = 4c_p G / K$ . Using

$\Omega_1 = 4(\tau/\rho) J' / D_\phi$ , the remaining parameters can be taken as temperature

dependent material parameters. They are:

$C_{ijkl}^0, \alpha_{kl}, \alpha, V_0, m, n, c_p, \rho, \tau, K, K', J'$ , and  $D_\phi$ .

Setting the variation of the action to zero yields:

$$\rho \frac{\partial^2 u_i}{\partial t^2} = \sigma_{ij,j} - F_i$$

$$\rho \frac{\partial \tilde{u}}{\partial t} = (K' \tilde{u}_{,i})_{,i} - \frac{1}{2} \frac{\partial K'}{\partial \tilde{u}} \tilde{u}_{,i} \tilde{u}_{,i} + \frac{\partial \sigma_{ij}}{\partial \tilde{u}} \dot{\epsilon}_{ij}, \text{ and}$$

$$\rho \frac{\partial \tilde{v}}{\partial t} = (J \tilde{v}_{,i})_{,i} - \frac{1}{2} \frac{\partial J'}{\partial \tilde{v}} \tilde{v}_{,i} \tilde{v}_{,i} - V'_{DW}(\phi) \frac{\partial \phi}{\partial \tilde{v}} - \int \frac{\partial \sigma_{ij}}{\partial \tilde{v}} d\epsilon'_{ij}.$$

Note that  $\frac{\partial \sigma_{ij}}{\partial \tilde{v}} = \frac{\partial \sigma_{ij}}{\partial \phi} \frac{\partial \phi}{\partial \tilde{v}} \frac{\partial \tilde{v}}{\partial \tilde{v}} = C_{ijkl}^0 g'(\phi) [\epsilon_{kl} - \alpha_{kl}(T)(T - T_R) - \epsilon_{kl}^p] [\sqrt{\phi/(\tau/\rho)}] \Omega_i$

## References

- [1] X.-P. Xu and A. Needleman, J. Mech. Phys. Solids 42, 1397 (1994); E. Johnson, Int. J. Fract. 57, R27 (1992).
- [2] J. Fineberg and M. Marder, Phys. Rep. 313, 1–108 (1999); K. Broberg, Cracks and Fractures (Academic, New York, 1999); L. B. Freund, Dynamic Fracture Mechanics (Cambridge University Press, Cambridge, 1990).
- [3] L.B. Freund, Dynamic Fracture Mechanics, Cambridge University Press, Cambridge, England, 1990
- [4] E. Sharon and J. Fineberg, Nature (London) 397, 333, 1999
- [5] T. Cramer et al., Z. Metallkd. 90, 675 1999. Physical Review Letters, 85, 788, 2000
- [6] K. Ravichandar, W.G. Knauss, Int. J. Fract. 25, 247 1984.
- [7] Brice Cassenti, Alexander Staroselsky, Gaynath Fernando, “A Physics Based Lagrangian for the Heat-Diffusion Equation”, Accepted for publication in Philosophical Transactions Letters, 2013
- [8] Alain Karma, David A. Kessler, and Herbert Levine, “Phase-Field Model of Mode III Dynamic Fracture”, Physical Review Letters, 87, No. 4, July 23, 2001.
- [9] Alain Karma, Vincent Hakim, “Laws of Crack Motion and Phase-field Models of Fracture”, Journal of the Mechanics and Physics of Solids, 57, October 21, 2008.
- [10] A. Karma, A. E. Lobkovsky, “Unsteady Crack Motion and Branching in a Phase-Field Model of Brittle Fracture,” Physical Review Letters, 92, 24, June 2004
- [11] M. Ortiz, Q. Yang, L. Stainier, “A variational formulation of the coupled thermo-mechanical boundary-value problem for general dissipative solids”, Journal of the Mechanics and Physics of Solids, 54, August 22, 2005.
- [12] Cassenti, B. and B. Murray, A Physical Basis for the Development of Constitutive Models, in Advances in Inelastic Analysis, edited by S. Nakazawa, K. William and N. Rebelo, AMD-Vol. 88 and PED Vol. 28, The American Society of Mechanical Engineers, New York, pp 75-86, 1987.
- [13] Cresson, J., I. Greffa and P. Inizan, Lagrangian for the Convection-Diffusion Equation, <http://hal.archives-ouvertes.fr/docs/00/65/18/26/PDF/arxiv-cresson-greff-inizan.pdf>, 14 December 2011.
- [14] M. Abramowitz and I. A. Stegun, Handbook of Mathematical Functions: with Formulas, Graphs, and Mathematical Tables, National Bureau of Standards, Applied Mathematics Series 55, Issued June 1964, Ninth Printing, November 1970, with corrections
- [15] Richard Haberman, Applied Partial Differential Equations with Fourier Series and Boundary Value Problems. 4th Edition, 2004
- [16] W. Michael Lai, Introduction to Continuum Mechanics, 4<sup>th</sup> Edition, 2010

- [17] Gerald Recktenwald, Numerical Methods with Matlab Implementation and Application, 2000
- [18] G.P. Cherepanov, Mechanics of Brittle Fracture, U.S. National Bureau of Standards, 1974
- [19] D.P. Rooke, D.J. Cartwright, Compendium of stress intensity factors. HMSO Ministry of Defense, Procurement Executive, 1976
- [20] M. Isida, "Effect of Width and Length on Stress Intensity Factors of Internally Cracked Plates Under Various Boundary Conditions", Int. J. Frac. Vol. 7, No. 3 (1971), pp. 301-316.